



Production technology of late Roman decorated tableware from the Vesuvius environs: Evidence from Pollena Trocchia (Campania region, Italy)

Chiara Germinario¹  | Giuseppe Cultrone²  | Alberto De Bonis^{3,4}  |
 Girolamo F. De Simone⁵  | Michele Gorrasi¹ | Francesco Izzo³  |
 Alessio Langella^{1,4}  | Caterina S. Martucci⁶ | Mariano Mercurio^{1,4}  |
 Vincenzo Morra^{3,4}  | Christopher R. Vyhna⁷  | Celestino Grifa^{1,4} 

¹Dipartimento di Scienze e Tecnologie, Università degli Studi del Sannio, Benevento, Italy

²Departamento de Mineralogía y Petrología, Universidad de Granada, Granada, Spain

³Dipartimento di Scienze della Terra, dell'Ambiente e delle Risorse, Università degli Studi di Napoli Federico II, Napoli, Italy

⁴CRACS, Center for Research on Archaeometry and Conservation Science, Napoli, Italy

⁵Dipartimento Storia Culture Civiltà, Alma Mater Studiorum Università di Bologna, Bologna, Italy

⁶Museo Archeologico Nazionale di Napoli, Ministero per i Beni e le Attività Culturali, Napoli, Italy

⁷Science Department, The Thacher School, Ojai, California

Correspondence

Celestino Grifa, Dipartimento di Scienze e Tecnologie, Università degli Studi del Sannio, Via De Sanctis snc, 82100 Benevento, Italy. Email: celestino.grifa@unisannio.it

Scientific editing by Kevin Walsh

Funding information

Università degli Studi del Sannio, Grant/Award Number: FRA 2015 CG; Junta de Andalucía, Grant/Award Number: MAT2016-75889-R

Abstract

The northern slope of Mt. Vesuvius contains some interesting archaeological sites, including the site discovered in the town of *Pollena Trocchia*, where the remains, dated to between the 79 and 472 CE eruptions, document the transition from the Roman to late Roman cultural and socioeconomic settings. Profound changes occurred in this time interval, which can be inferred from changes in the ceramic manufacturing processes. Common wares, as the most widespread ceramic class in the archaeological record, are a useful example that illustrates this technological transformation. Seventeen samples of tableware, distinguished into three ceramic classes according to the method of slip application (i.e., Slipped Ware, Painted Ware “a straccio,” and Painted Ware), were analyzed. The results highlight the use of high-CaO clayey raw materials compositionally similar to Apennine clayey deposits. The clay bodies were occasionally tempered with sandy-silt materials composed of volcanic grains with lesser amounts of siliclastic fragments. Firing temperatures ranged from 800 to 950°C, as suggested by quantitative X-ray powder diffraction and microstructural analyses combined with colorimetric measurements of the ceramic bodies. Micro-Raman analyses performed on slips revealed the use of ochre for decorating the vessels; it was applied in a different way, representing an actual technological change.

KEYWORDS

ceramic technology, decorated pottery, late Roman period, Pollena Trocchia, Vesuvius environs

1 | INTRODUCTION

Late Antiquity (or the late Roman period) marked the transition from the Classical Period to the Middle Ages. The common thinking recognizes the period as one of profound instability that signified the beginning of one of the most important social and economic collapses

in history; these changes can also be clearly seen in the technological transformations occurring in ceramic materials production. The late Roman ceramic facilities, in fact, record a reorganization of ceramists into local workshops which resulted in a reduction of large-scale productions as well as a modification of the manufacturing technology (Arthur, 2007). The traditional fine ware from the Republican and

Early Roman Imperial ages, with its mass-production technology and large and standardized repertoire, declined, giving rise to simply and roughly decorated common wares (Arthur, 2007). From the middle of the 1st century CE, workshops widespread in the Italian territories stopped producing the famed traditional fine ware pottery (e.g., Red Slip Ware or *Terra Sigillata Italica*), due to its higher costs of production compared with African fine wares (African Red Slip Ware, hereafter ARS). ARS continued to reach western Italian harbors until the 5th century CE (De Simone et al., 2012; Wickham, 1998) from northern Africa, where most was produced (Mackensen & Schneider, 2002). ARS initially imitated the most popular shapes of the Italian and Gaulish *Terra Sigillata* using a simpler and cheaper technology. This economic reason and, mostly, the fact that the ARS constituted the accompany charge for the African oil and grain, determinate the success and development of this ceramic industry from the early Empire to the collapse of the western Empire up to the 7th century CE (De Simone et al., 2012; Wickham, 1998). Studies on the distribution of ARS and commercial trade routes during the late Roman period attest to the presence of such tableware both in eastern and western Mediterranean sites. This pottery also reached the Italian sites, as proved by their constant occurrence (together with pottery from local productions), in late Roman layers of the Italian main cities (e.g., Rome, Ostia, Naples, etc.) and small inland villages (Bowersock, Brown, & Grabar, 1999; Wilson, Schörle, & Rice, 2012).

Despite a reasonable standardization of the morphological catalogue, the technological properties of the Italian decorated wares started to be produced in the late Roman period seem to reflect less consistency in their production process (De Simone et al., 2012; Germinario, Cultrone, et al., 2018; Germinario et al., 2019; Santoriello & Siano, 2018; Martucci, Boemio, Trojsi, & De Simone, 2012). Archaeological excavations, which recovered a large amount of this pottery from the late Roman archaeological sites in Campania, highlight a gradual change in ceramic technology, evident in both the morphological repertoire and the process of decorating the vessels, where esthetic features started to succumb to functional or practical ones (Arthur, 2007). This tableware can be organized in three principal ceramic classes, namely Slipped Wares, Painted Ware “a straccio” and Painted Wares, which are distinguished by their different shape repertoire and decorative patterns.

The present paper is focused on the study of these productions unearthed from a Roman villa with baths in the property known as *Masseria De Carolis* (now “Parco Europa”) in the town of *Pollena Trocchia* (near modern-day Naples, Italy), an outstanding archaeological site located in the area north of Mt. Vesuvius, a territory quite interesting, in archaeological terms, for the study of ceramics production and economic dynamics during the late Roman period. The site is chronologically and stratigraphically constrained by the deposits of the 79 and 472 CE volcanic eruptions, and is the object of a wide multidisciplinary research program named the “Apolline Project” (De Simone & Macfarlane, 2009).

This study aims to characterize, from the archaeometric point of view, the production of late Roman common wares and to

define, to the extent possible, their technological properties. To this end, each measurable feature of ceramic bodies was evaluated by means of a multianalytical approach and compared to the established chronology to evaluate the technological changes in pottery production, assuming that “technology” is not only what pertains to the preparation of the ceramic paste and firing conditions, but, in broader terms, everything related to the realization of a ceramic artefact in each stage of its production, including its decoration.

2 | GEOLOGICAL AND VOLCANOLOGICAL BACKGROUND

The city of *Pollena Trocchia* is located just behind the Bay of Naples coastline, an area dominated by the presence of the two volcanic complexes of the Somma-Vesuvius to the east and of the Phlegraean Fields in the western sector (Figure 1a).

Pollena Trocchia is situated on the northern slope of the Somma-Vesuvius complex (Figure 1a) that strongly influenced the history of inhabited settlements located here. As is widely known, the eruptive history of Mt. Vesuvius is characterized by violent Plinian and sub-Plinian eruptions followed by long periods of inactivity. The oldest volcano, Mount Somma, collapsed after four main Plinian events occurred between 18.3 ka and the year 79 CE (Barberi, Davis, Isaia, Nave, & Ricci, 2008), forming a summit caldera in which the youngest edifice of the Vesuvius volcano developed (Cioni, Santacroce, & Sbrana, 1999; Scarpati, Perrotta, & Luongo, 2009). After the last Plinian event in 79 CE, two sub-Plinian events occurred in 472 CE and 1631 CE. After the large sub-Plinian 472 CE event, the first eruption took place in the summer of 512 CE, and then, weak, low-energy, effusive, and explosive eruptions continued up to the 1631 CE eruption. Since then, the volcanic activity changed: Vesuvius entered into an open conduit phase, and violent, effusive-explosive events took place until the last episode in 1944 (Arrighi, Principe, & Rosi, 2001). The volcano has since remained in a new phase of quiescence (Barberi et al., 2008).

All volcanic events erupted ultrapotassic, silica-undersaturated and leucite-bearing products (Conticelli et al., 2010). Lapilli and ash fallout, formed during the phreatic or phreatomagmatic initial phase of Plinian and sub-Plinian eruptions, had their principal dispersion axis eastward, where these deposits are widespread. The geologic deposits of pyroclastic flows (caused by the collapse of a sustained eruptive column), and lahars (resulting from rain-mobilized ash into mudflows during and after eruptions), crop out in greater thicknesses around the volcanic slopes (Scarpati et al., 2009). Pyroclastic deposits emplaced by the Somma-Vesuvius eruptions strongly contributed to the destruction and abandonment of inhabited areas around the volcano, such as *Masseria De Carolis*, which was buried by debris flow deposits of the 472 CE eruption and successive Medieval eruptions. In the area near *Pollena Trocchia*, the stratigraphic sequence is characterized from the bottom upward by a pre-79 CE soil and the products of prehistoric eruptions, followed by a stratified ash deposit

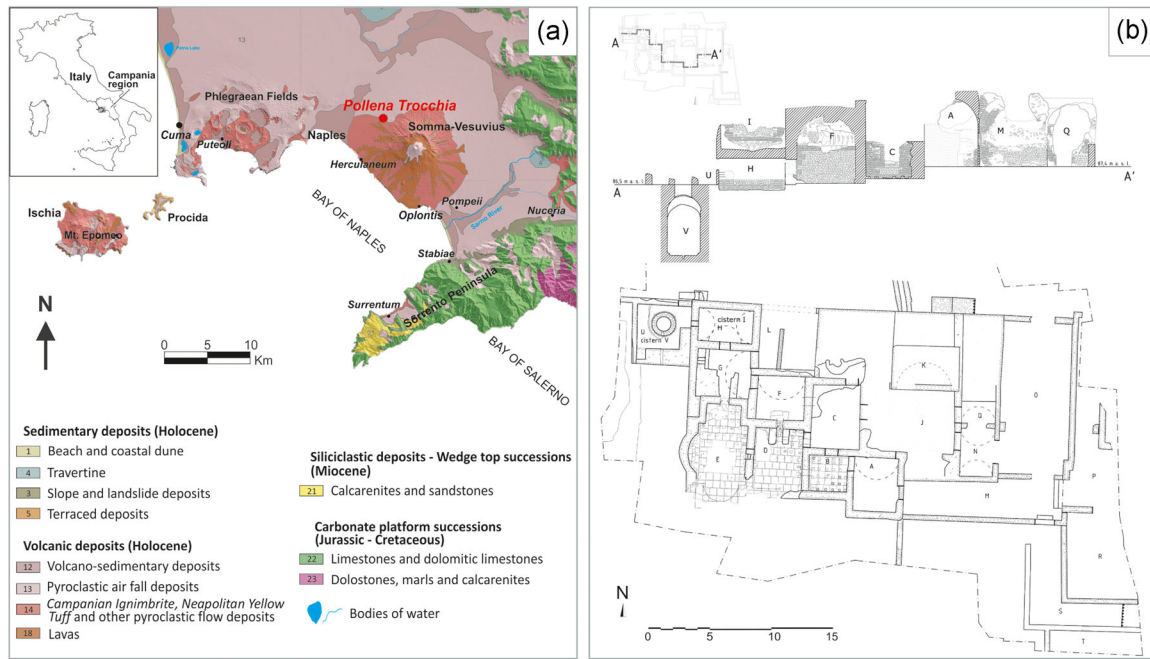


FIGURE 1 (a) Geological sketch map of the Bay of Naples (modified by De Bonis et al., 2016); (b) site plan and west-east section cross-section of *Masseria De Carolis* archaeological site in *Pollena Trocchia* (modified from De Simone et al., 2018). The letters are related to the different rooms here unearthed (a detailed description is reported in De Simone et al., 2018) [Color figure can be viewed at wileyonlinelibrary.com]

of the 79 CE Plinian event (Scarpati, Perrotta, & De Simone, 2016). A several meters thick deposit emplaced during the 472 CE eruption follows, consisting mostly of thick volcanoclastic beds of scoria fall and a stratified ash deposit emplaced from a pyroclastic flow. A thin, pinkish paleosol separates this deposit from the products of the 512 CE eruption (Scarpati et al., 2016).

The nearby Phlegraean Fields volcanic area is characterized by the presence of monogenetic vents, few lava bodies and large, caldera-forming ignimbrites, which emplaced huge volumes of pyroclastic rocks and very sporadic lava flows. The eruptive events resulting in the Campanian Ignimbrite (39 ka) and the Neapolitan Yellow Tuff (15.4 ka), emplaced the largest amounts of products (about 200 and 40 km³ of magma dense rock equivalent, respectively; Forni, Degruyter, Bachmann, De Astis, & Mollo, 2018). From a petrological point of view, The products of the Phlegraean Fields, including the islands of Ischia and Procida, belong to shoshonitic series, among which trachytes are the most common lithotype (Melluso, de' Gennaro, Fedele, Franciosi, & Morra, 2012).

The geological framework of the Campanian region also accounts for the presence of clayey deposits, mainly associated with siliciclastic and/or carbonate marine sedimentary formations, which were exploited for ceramics production since ancient times. Some clays belong to pre-orogenic domains of Lower Cretaceous–Upper Miocene (e.g., *Argille Varicolori*) deposits, while other high-CaO clayey deposits are found in more recent (Miocene–Pliocene) wedge-top basin domains (De Bonis et al., 2013; Grifa et al., 2009). It is worth noting that marine clayey sediments can also be found in the volcanic framework of the Ischia island, cropping out on the northern side of Mt. Epomeo, due to uplift after the Green Tuff

eruption (55 ka; e.g., De Bonis et al., 2013). Campanian clayey materials can also be found in Quaternary alluvial/lacustrine sediments, as in the floodplains of major rivers (e.g., Volturno, Sarno, Sele, Alento) or in strongly weathered pyroclastic deposits, where the argillification resulted in plastic clayey materials also used in the today's traditional ceramic manufacture (De Bonis, Cultrone, Grifa, Langella, & Morra, 2014).

3 | ARCHAEOLOGICAL SETTING

The Roman villa with baths of *Masseria De Carolis* in the town of *Pollena Trocchia* (Figure 1a) is one of several interesting archaeological sites located on the northern slopes of Somma-Vesuvius volcanic complex. This site represents one of the best examples of reoccupation of the northern Vesuvian environs after the Pompeii eruption of 79 CE and is particularly significant for two reasons: (a) it is stratigraphically constrained between geologic deposits of the two volcanic eruptions in 79 and 472 CE (Scarpati et al., 2009) within the late Roman period; and (b) it is located on the northern slope of the volcano with ready access to both coastal and inland areas.

After its initial discovery in February of 1988, the site was abandoned and again explored since 2006, when archaeological surveys unearthed a building with baths (Figure 1b) built on pyroclastic layers of the 79 CE eruption and covered by pyroclastic flows of the so-called “Pollena” (472 CE) and later eruptions (Martucci et al., 2012). The archaeological evidence brought to light so far interprets the rooms as private baths (Figure 1b, rooms A to K) of a

sizeable villa (Figure 1b, rooms P and R) which extends towards the east, and which was likely built at the end of the 1st/beginning of the 2nd century CE, and which remained in use for at least two centuries (De Simone, Castaldo, & Sannino, 2018). Debris found along the walls in the northern area of the villa suggested that, probably after an earthquake, part of the building collapsed and the rooms were then used as a cemetery and dump. The rest of the villa appears to have been in use up to the 472 CE eruption, when it was almost completely buried (De Simone et al., 2018). Additionally, archaeological data suggest that the site was immediately and partially resettled after the 472 CE eruptive event and until later eruptions in 505 or 512 CE, when the site was completely buried and definitively abandoned (De Simone et al., 2018).

4 | CERAMIC MATERIALS

During the excavations of the villa, a large amount of pottery dating from the 2nd to the 5th century CE was unearthed, providing a clear snapshot of the production and circulation of pottery in a quite narrow timeframe (De Simone et al., 2012). In particular, late Roman local pottery from the 3rd to 5th century CE are the most commonly used types for the preparation and consumption of food and beverages and indicate a domestic and convivial occupation of the site (Martucci et al., 2012). Minor amphorae and lamps, and imported ARS pottery, African Cooking ware, and scarce Pantellerian and Eastern productions were also unearthed (De Simone et al., 2012; Martucci et al., 2012).

Late Roman pottery produced in central-southern Italy from the mid-3rd to the 6th centuries CE is also well represented in the archaeological layers, constituting a sort of cultural and technological “*koine*” due to the similar typological and stylistic features (Martucci et al., 2018; Soricelli, 2015). Late Roman common wares started to integrate into the market dominated by ARS (Bonifay, 2014) and organized into a rather standardized morphological repertoire evident in the coastal and inner Campanian territories (De Simone et al., 2012; Martucci et al., 2012; Martucci, De Simone, & D'Italia, 2014; Martucci et al., 2018; Santoriello & Siano, 2018). Thus, in the Campania region, these types of pottery also served as evidence of the sharing of technologies and ideal topological models throughout the region (De Simone et al., 2012; Martucci et al., 2012).

The above-mentioned late Roman pottery can be classified, on the basis of the surface treatment and decoration styles, in: (a) Slipped Ware (SW), (b) Painted Ware “a straccio” (PWS) and (c) Painted Ware (PW).

The classification scheme (after Martucci et al., 2018) provided the following descriptions:

- SW are those vases covered by a slip applied by immersion.
- PWS are the vases on which the whole external surface was colored by using a brush or a cloth/sponge soaked in a solution of water plus pigment.

- PW are those vessels on which the color was applied by a brush for creating decorative patterns.

Hereafter the most important features of each ceramic class, which are the object of the present research, are reported.

4.1 | Slipped ware

Starting in the mid-3rd century CE, a ceramic colored pottery known in the literature by the name SW (alternatively as Color Coated Ware/*C eramique engob ee/Ingobbiate*) was produced throughout the Italian peninsula (Fontana, 1998); in the Campania region, production centers have been identified in the *ager Falernus* and near Mt. Vesuvius (Arthur & Soricelli, 2015; De Simone et al., 2012; Martucci et al., 2018; Soricelli, 2015). This ceramic class was also known as *Cascano ware* from the locality in the *Ager Falernus* where production kilns have been identified (Arthur, 1987). Its first occurrence in Campanian archaeological records dates to the mid-3rd century CE, as shown by recent discoveries in Somma-Vesuvius contexts, and the archaeological evidence from northern Campania documents production and circulation of this pottery into the 5th century CE (Mukay & Aoyagi, 2014; Soricelli, 2015). However, in the villa with baths in *Pollena Trocchia*, this class of pottery is residual in the archaeological contexts at the end of the 5th century CE and reflects dumping activity (Martucci et al., 2018).

This ceramic class is characterized by a red/brown slip that covers both the internal and external surfaces of the vessel (Figure 2), occasionally exhibiting a metallic luster. Sometimes decorative patterns made by rouletting are present (Martucci et al., 2012, 2018). Potter's fingerprints are often visible at the points where the vase was held during immersion in the slip.

SW seems to continue the repertoire of the former Thin Walled Pottery, integrating the tableware set of the ARS with mostly closed shapes such as large bowls, vessels to serve beverages, cups, small bowls and jugs.

For this study, four specimens of SW, encompassing both open and closed shapes (Table 1 and Figure 2) were analyzed. Hard, fine or medium-textured ceramic bodies characterized the samples (Martucci et al., 2018); moreover, samples MDC 38/17 and MDC 49/4 show a zoning with a different color of the ceramic matrix in the innermost part.

4.2 | Painted ware “a straccio”

From the mid-4th century, the production of the PWS started with a shape repertoire encompassing and imitating the African Red Slip Ware D (ARS-D; Soricelli, 2015). The interior and the upper part of the exterior of the vases (usually the rim) were covered by red/orange/brown colored slip (Figure 2). The slip was rougher, and applied more thinly and less homogeneously with respect to the slip of the SW (Martucci et al., 2018). The marks of the instrument

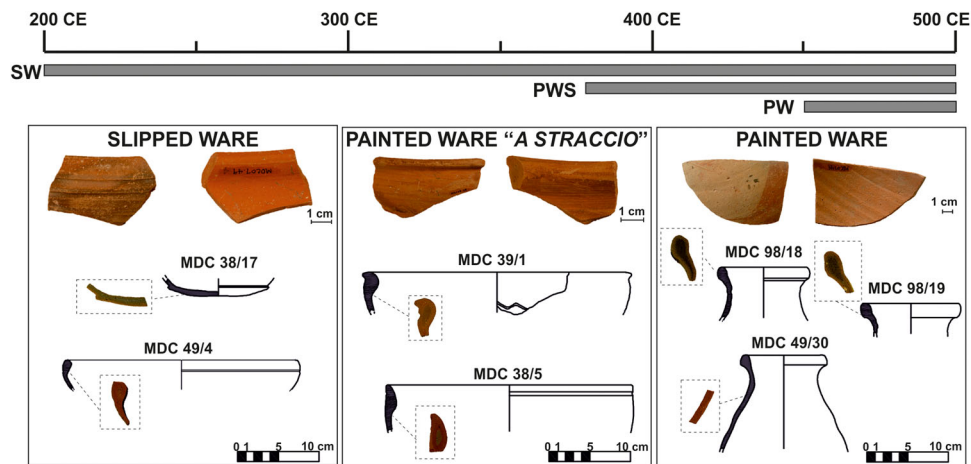


FIGURE 2 Ceramic shapes of SW (samples MDC 38/17, MDC 49/4), PWS (samples MDC 38/5, MDC 39/1), and PW (samples MDC 49/30, MDC 98/18, MDC 98/19) with relative chronology. Pictures of corresponding fresh-fractured surfaces are also reported. The scale is only referred to the reconstructions of ceramic shapes. PW, painted ware; PWS, painted wares “a straccio”; SW, slipped ware [Color figure can be viewed at wileyonlinelibrary.com]

(i.e., brush or cloth) employed in this operation are often evident on the surface of the vases.

The change in the method of applying the slip to this pottery likely accompanies the change of the shape repertoire. The SW repertoire encompasses mostly small artefacts, whereas the PWS repertoire mostly includes large bowls (Martucci et al., 2018). In particular, PWS encompasses a new type of deep bowl/basin with either an internal thickened or flanged rim (Soricelli, 2015).

Four fragments of PWS, consisting of multifunctional bowls or basins (Table 1 and Figure 2) were selected for analysis. The

structure of hard ceramic bodies is characterized by fine- or medium-grained a-plastic inclusions scattered in the clayey matrices (Martucci et al., 2018), sometimes zoned.

4.3 | Painted ware

During the 5th century, another change in the shape repertoire and in the process of coloring the vessels was observed. In fact, up to the 7th century CE, together with the multifunctional basin typical of the

TABLE 1 Archaeological information of analysed SW, PWS, and PW samples

Group samples	ID sample	Horizontal provenance (trench/room)	Vertical provenance (US)	Shape	Type	Sample chronology
SW	MDC 38/17	Trench 5/Room f	US 38	Closed		3rd-end 5th
	MDC 38/21	Trench 5/Room f	US 38	Closed		3rd-end 5th
	MDC 49/4	Trench 5/Room f	US 49	Bowl		4th
	MDC 49/31	Trench 5/Room f	US 49	Jug		3rd-end 5th
PWS	MDC 38/5	Trench 5/Room f	US 38	Bowl	Carminiello 61	End 4th-end 5th
	MDC 38/6	Trench 5/Room f	US 38	Bowl	Carminiello 62	End 4th-end 5th
	MDC 38/19	Trench 5/Room f	US 38	Closed		End 4th-end 5th
	MDC 39/1	Trench 5/Room f	US 39	Bowl	Carminiello 60	End 5th
PW	MDC 38/16	Trench 5/Room f	US 38	Jug	Carminiello 98	Second half of 5th
	MDC 38/18	Trench 5/Room f	US 38	Closed		End 5th
	MDC 38/20	Trench 5/Room f	US 38	Closed		Second half of 5th
	MDC 38/22	Trench 5/Room f	US 38	Closed		Second half of 5th
	MDC 49/29	Trench 5/Room f	US 49	Closed		End 5th
	MDC 49/30	Trench 5/Room f	US 49	Closed		End 5th
	MDC 98/18	Trench 4	US 98	Jug	Carminiello 94	Second half of 5th
	MDC 98/19	Trench 4	US 98	Jug	Carminiello 94	End 5th
	MDC 282/48	Trench 7/Room h	US 282	Basin	Carminiello 67	End 5th

Note: The acronym used for the ID samples (MDC) is related back to the discovery site of *Masseria de Carolis*.

Abbreviations: PW, painted ware; PWS, painted wares “a straccio”; SW, slipped wares.

PWS, production evolved to the manufacturing of mostly closed shapes, primarily jugs, characterized by the presence on the outer surface of the vessels of very simple but intentional decorative patterns, made with light red to very dark gray brush strokes (Figure 2). PW had a repertoire completely different from the ARS, although the latter was still present in the market with only open shapes. For this ceramic class, nine samples, occasionally with a zoned ceramic body, were selected for analysis (Table 1).

5 | ANALYTICAL TECHNIQUES

For this study, a total number of 17 fragments of the different color coated productions of tableware were selected as representative for the archaeometric investigation (Table S1). Color, fabric, decoration, and shape were the macroscopic features that permitted sample selection.

Mineralogical and textural features of ceramic pastes were investigated in thin sections by means of polarized light microscopy (PLM; Quinn, 2013) with a Nikon Eclipse 6400 POL microscope. Observations were recorded over a representative area of each sample and micrographs were acquired in both plane-polarized and crossed-polarized light to accurately discriminate each component of ceramic paste (a-plastic inclusions, matrix, pores). Image analyses were performed using ImageJ software, which allowed for the evaluation of grain size distribution (hereafter GSD) by using the minimum Feret (mF) value to calculate the Krumbain ϕ ($\phi_{mF} = -\log(mF)$) and circularity ($C = 4\pi(A/p^2)$, where A = area, p = perimeter) values to quantitatively characterize the shape of particles (Germinario, Grifa, & Di Maggio, 2019; Grifa et al., 2013). Circularity values describe the shape of a particle along a continuum from $C = 0$ (a perfectly linear feature) to $C = 1$ (a perfect circle; Izzo et al., 2018). Density histograms of textural and shape parameters were obtained using R Development Team software (2008).

Quantitative evaluation of the color of ceramic bodies and slips was performed by colorimetric measurements on fresh-fractured surfaces using a portable Konica Minolta CM-700d spectrophotometer (De Bonis et al., 2017). CIE illuminant D65 (simulating daylight with a color temperature of 6,504 K) was selected for determining chromatic coordinates (CIE $L^*a^*b^*$ values) in the 400–700 nm wavelength range. The illumination was provided by a pulsed xenon lamp with UV cut filter, while a silicon photodiode array detected and measured both incident and reflected light (Germinario, Cultrone, et al., 2018). Where both the rims and cores of zoned ceramic samples were of sufficient thickness to allow for adequate discrimination given the 3 mm spot size of the instrument, the colors of both were measured. Colorimetric measurements have been correlated with porosimetric and mineralogical features of ceramic pastes to estimate the firing temperatures and evaluating the influence of mineralogical transformation on the color of the ceramic body and microstructures.

The analysis of porosity was carried out by free, forced water absorption and drying tests, following Normal and RILEM standard

procedures (RILEM 1980; NORMAL 7/81; NORMAL 29/88). Although cylindrical or cubic shaped standard test pieces of 5 cm were not available, it has been demonstrated that hydric tests performed on ceramic fragments give reliable results (Cultrone, Molina, & Arizzi, 2014). These hydric tests were performed only on specimens weighing more than 10 g (dry weight). Free water absorption (A_b), forced water absorption (A_f); saturation coefficient (S), drying index (Di), apparent density (ρ_b), skeletal (real) density (ρ_{sk}) and open porosity (Po) have been determined by these hydric tests.

On lightweight samples (<10 g) the porosity and the pore size distribution (hereafter PSD) were measured by means of mercury intrusion porosimetry (MIP) using a Micrometrics AutoPore III 9410 apparatus, exerting a maximum pressure of 414 MPa and measuring pores with dimensions ranging from 0.003 to 360 μm . Along with the open porosity (Po_{MIP}), MIP allowed for the determination of the specific surface area. On specimen MDC 38/17, porosity was not determined due to the scarce amount of available sample.

Mineralogical composition was determined by X-ray powder diffraction (XRPD) on very fine powders (grain size <10 μm) obtained using a McCrone micronizing mill with agate cylinders and a wet grinding time of 15 min. An α - Al_2O_3 internal standard (1 μm , Buehler Micropolish) was added as 20% of each sample to perform quantitative analyses (Bish & Reynolds, 1989). XRPD patterns were collected with a Philips PW 1730/3710 diffractometer (CuK α radiation, 40 kV, 30 mA, curved graphite monochromator, 2θ scanning interval 3°–50°, step size = 0.020° 2θ , counting time 5 s per step) equipped with X-Pert data collector and X-Pert HighScore Plus software. Quantitative mineralogical data were obtained by combining Rietveld and reference intensity ratio methods using TOPAS 4.2 software (BRUKER AXS Company; Grifa et al., 2017), thus allowing the estimation of both crystalline and Low Ordered-Amorphous Phases (hereafter LO-AP). Atomic starting coordinates for identified crystalline phases were taken from literature (Inorganic Crystal Structure Database, 2014) whereas phases with partial or unknown crystal structure (i.e., LO-AP) were quantified by adding a “peaks phase” with the TOPAS software (Mercurio et al., 2016).

Observations of microstructures have been made via scanning electron microscopy (SEM) on freshly fractured and gold-coated fragments, whereas microchemical analyses on carbon-coated thin sections were performed using a Zeiss SEM EVO HD15 equipped with an Oxford Instruments microanalysis unit with an Xmax 80 EDS detector. Standard details that were utilized are reported in Germinario et al. (2019).

The chemical composition of ceramic pastes, a valuable parameter for the determination of provenance of raw materials (Maggetti, 2001), was obtained by using an X-ray fluorescence (XRF) AXIOS PANalytical Instrument on pressed powder pellets and reported as the content of major oxides (SiO_2 , TiO_2 , Al_2O_3 , Fe_2O_3 , MnO , MgO , CaO , Na_2O , K_2O , P_2O_5 in wt.%) and trace elements (Rb, Sr, Y, Zr, Nb, Ba, Cr, Ni, Sc, V, La, Ce in ppm).

Finally, particular attention was paid to the surface treatments that clearly signify changes in decoration over time. To this aim, microtextural and mineralogical analyses by using spectroscopic techniques

(Barilaro et al., 2005) were performed to determine the pigments and decorative techniques utilized. Mineralogical composition of the ceramic slips was investigated by μ -Raman spectroscopy. Representative samples, selected on the basis of the state of preservation of the slips, were analysed using a JASCO NRS-5100 μ -Raman dispersive spectrometer equipped with a near-infrared diode laser (785 nm). A collection time of 30, 60, or 90 s with one to three accumulations and a magnification of $\times 100$ were adopted. The 521 cm^{-1} peak of a silicon standard was employed for the calibration of laser beam. The Raman spectra were treated by applying both smoothing and baseline corrections using Spectra Manager II Software.

6 | RESULTS AND DISCUSSION

The above-mentioned analytical approach provides some insight into each respective part of the pottery production; this section aims at walking the reader through the pottery-making process from start to finish.

6.1 | Type of raw materials

The bulk chemical composition of pottery is considered important in determining the type of clay exploited for ceramic productions, considering the firing process as isochemical (Schwedt & Mommsen, 2007). In the analyzed samples, calcium content ranges from 8.4 to 17.3 wt% and has an inverse relationship with silica (54.8–61.4 wt%) and alumina (13.7–15.9 wt%) (Table 2). As a first approximation, the exploitation of high-CaO clays (hereafter HCC, containing a CaO content ≥ 6 wt%; De Bonis et al., 2013) can be inferred.

Additionally, a concentration of CaO >15 wt% characterized PWS samples (apart from sample MDC 39/1; Figure 3a; Table 2), which also showed higher concentration of Sr and lower concentrations of Rb, Zr, and Nb (Figure 3b–d and Table 2). It also should be noted that chemical composition of sample MDC 282/48 (PW) is consistent with that of PWS samples (Table 2). Such a high calcium concentration likely reflects the abundance of carbonates in the original clayey raw material, in the form of crystals and/or skeleton particles fossils.

On the other hand, the majority of SW and PW samples are chemically homogeneous (Figure 3a–d). They differ slightly from PWS samples for lower CaO and Sr, and higher SiO_2 , Al_2O_3 , Rb, Zr, Nb, and Ni contents (Table 2) likely due to compositional changes in the clay deposit. Only sample MDC 49/30 shows higher SiO_2 , and lower CaO contents (Table 2). Moreover, in sample MDC 38/19, a P_2O_5 content (1.41 wt%) exceeding the average value (0.51 wt%), likely suggests postdepositional alteration phenomena (Maritan & Mazzoli, 2004; Maritan, Angelini, Artioli, Mazzoli, & Saracino, 2009).

To identify the potential source of raw materials, compositional features of pottery were compared with those of clay deposits from the Campania region that were supposedly exploited for ceramic production (De Bonis et al., 2013, 2016). In particular, compositional

diagrams in Figure 3 show that the concentration of major oxides and trace elements of pottery are consistent with that of marine clay deposits outcropping extensively along the Campanian sector of the Apennine chain, and differing from the composition of the other main high-CaO clayey sources exploited from Ischia island, which are plotted for comparison (Figure 3). It appears that the main differences with Ischia clays consist in the content of trace elements concentration (Figure 3b–d), as the Ischia clays are clearly recognizable among the HCC samples from Campania region for their high Zr enrichment (>200 ppm), low Cr (<100 ppm), and high Nb (>20 ppm) contents (De Bonis et al., 2013). Thus, compositional features suggest the possible utilization of Apennine HCC, belonging to Miocene-Pleistocene basinal deposits that have represented one of the most widespread types of clayey raw material used in the productive centers of the region from ancient times until recent traditional productions (De Bonis et al., 2010, 2013, 2018; Grifa et al., 2009, 2018; Peña & McCallum, 2009a, 2009b; Scarpelli, Clark, & De Francesco, 2014).

6.2 | Mineralogy, texture, and porosity of ceramic bodies

A multi-analytical approach was adopted for investigating the ceramic bodies with the aim of (a) finding, if possible, any distinctive features for each ceramic class; (b) inferring meaningful information about the ceramic process and production technology, namely the mix-design of the pottery and its pore system.

Textural differences are observed in the samples, but they are not associated with the SW, PWS, and PW categories of the pottery. Samples MDC 38/5, MDC 38/6, MDC 38/19 (PWS), MDC 38/21 (SW), and MDC 282/48 (PW), in fact, are characterized by a seriate grain-size distribution of a-plastic inclusions composed of fine quartz, feldspar, mica, and calcite (Table 3 and Figures 4a,b), the latter occurring as microcrystals, relicts of fossils (Figure 4c) and a secondary phase filling the pores as highly birefringent material. Only in samples MDC 38/5 and MDC 282/48 is calcite still preserved among the residual grains, although partially decomposed. GSD ranges from very fine silt (0.005 mm) to fine sand (0.198 mm) (average $\phi_{mF} = 5.54$, ~ 0.021 mm), showing a moderate well sorting (average $\sigma\phi = 0.62$; Table 3; Figure 4d).

The remaining samples, instead, showed bimodal pastes containing coarser volcanic fragments, associated with occasional siliciclastic grains, along with residual a-plastic inclusions (Figures 4e,f). Volcanic grains consist of alkali-feldspar, plagioclase, clinopyroxene, juvenile volcanics, biotite, hematite, olivine, garnet (Figure 4g) and leucite-bearing scoriae. Minor grains of quartz, detrital arenaceous and/or silty fragments represent the siliciclastic counterpart. In the specimen MDC 49/4 grog was also observed (Table 3).

Particles are moderately sorted (average $\sigma\phi = 0.76$) and GSD varied from very fine silt (0.004 mm) to coarse sand (0.903 mm; Table 3). The distribution of ϕ_{mF} curve is clearly bimodal, where coarser particles have sandy-silty dimension (2.5–4 ϕ_{mF} ; Figure 4h) and high circularity (average $C = 0.76$; Table 3).

TABLE 2 Chemical composition of ceramic samples obtained by X-ray fluorescence analyses, expressed in terms of major oxides (wt% recalculated to 100% on a LOI-free basis) and trace elements (ppm)

Ceramic class	ID Sample	SiO ₂	Ti- O ₂	Al ₂ - O ₃	Fe ₂ O ₃	MnO	MgO	CaO	Na ₂ O	K ₂ O	P ₂ O ₅	Rb	Sr	Y	Zr	Nb	Ba	Cr	Ni	Sc	V	La	Ce
SW	MDC 38/17	58.95	0.73	14.70	6.42	0.09	3.32	11.33	0.68	3.33	0.45	188.4	321.4	31.9	164.9	19.0	376.1	151.1	60.6	17.1	141.8	35.3	63.0
	MDC 38/21	56.67	0.73	14.78	6.20	0.09	3.20	13.98	0.91	3.05	0.40	149.6	441.2	32.1	170.5	16.4	388.9	124.1	45.0	18.8	85.5	35.2	59.8
	MDC 49/4	56.17	0.73	14.61	6.45	0.10	3.24	14.72	0.71	3.02	0.26	197.2	395.4	33.0	167.5	17.7	363.9	138.9	61.1	23.4	106.4	40.4	70.7
	MDC 49/31	56.55	0.72	14.55	6.37	0.10	3.11	14.46	0.68	3.10	0.34	195.7	378.5	34.4	168.1	18.1	383.4	145.9	58.6	24.9	144.0	40.6	64.2
	Average	57.08	0.73	14.66	6.36	0.10	3.22	13.62	0.75	3.12	0.36	182.7	384.1	32.9	167.8	17.8	378.1	140.0	56.3	21.1	119.4	37.9	64.4
σ	1.26	0.01	0.10	0.11	0.01	0.08	1.56	0.11	0.14	0.08	22.4	49.5	1.1	2.3	1.1	10.8	11.7	7.6	3.7	28.4	3.0	4.6	
PWS	MDC 38/5	55.40	0.71	13.67	5.87	0.08	2.88	17.30	0.67	3.05	0.36	142.5	471.6	30.1	155.4	15.0	374.0	122.3	44.2	20.4	134.9	31.0	63.8
	MDC 38/6	55.78	0.72	13.81	5.93	0.08	3.10	16.17	0.89	3.01	0.50	137.6	478.9	31.0	155.8	14.1	347.8	132.1	45.1	18.0	111.3	36.1	65.7
	MDC 38/19	54.84	0.72	14.43	6.01	0.08	3.44	15.09	0.93	3.06	1.41	149.3	565.4	28.6	144.7	11.3	349.4	132.7	54.5	19.7	131.5	37.4	59.0
	MDC 39/1	59.87	0.68	14.04	5.74	0.08	3.20	12.09	0.84	3.10	0.36	156.1	392.5	30.2	171.0	17.6	402.2	116.5	44.5	18.4	109.1	35.8	61.2
	Average	56.47	0.71	13.99	5.89	0.08	3.16	15.16	0.83	3.06	0.66	146.4	477.1	30.0	156.7	14.5	368.4	125.9	47.1	19.1	121.7	35.1	62.4
σ	2.30	0.02	0.33	0.11	0.00	0.23	2.24	0.11	0.04	0.51	8.1	70.7	1.0	10.8	2.6	25.6	7.9	7.9	5.0	1.1	13.4	2.8	2.9
PW	MDC 38/16	60.75	0.73	15.46	6.20	0.10	2.81	9.48	0.91	3.22	0.32	164.5	313.9	35.3	194.3	20.6	409.4	123.3	48.5	20.3	96.6	34.4	69.5
	MDC 38/18	58.67	0.72	14.75	6.18	0.10	3.04	11.98	1.06	3.21	0.30	161.8	424.5	31.6	195.3	20.3	476.2	122.5	45.0	22.1	107.3	33.0	57.1
	MDC 38/20	56.85	0.75	14.93	6.28	0.08	3.34	13.19	0.87	3.27	0.45	154.1	514.9	31.4	164.3	16.7	413.1	130.6	47.6	21.9	125.1	39.2	68.5
	MDC 38/22	56.66	0.72	14.53	6.22	0.08	3.30	13.86	0.84	3.44	0.35	153.7	534.1	30.8	155.9	15.4	400.6	123.7	44.9	23.4	110.8	34.1	64.2
	MDC 49/29	57.58	0.76	15.14	6.29	0.09	3.28	12.33	0.88	3.27	0.38	154.7	460.4	31.7	165.1	17.4	392.4	141.4	47.1	18.7	142.1	37.3	73.6
	MDC 49/30	61.44	0.72	15.91	5.77	0.08	2.93	8.36	1.06	3.39	0.34	188.9	294.8	33.4	196.2	22.8	469.7	114.6	45.8	19.7	83.4	46.9	63.3
	MDC 98/18	56.15	0.72	15.01	6.19	0.10	3.16	13.69	0.95	3.10	0.93	164.3	449.5	32.2	179.3	20.8	421.9	122.4	45.2	20.0	132.6	35.8	74.3
	MDC 98/19	57.52	0.74	15.14	6.06	0.10	3.25	12.27	0.96	3.23	0.72	163.6	435.4	33.9	189.2	21.4	435.9	122.4	44.0	22.1	132.5	45.3	79.3
	MDC 282/48	55.07	0.75	14.09	6.15	0.09	2.94	16.41	0.59	3.02	0.88	136.8	462.9	31.1	154.2	14.9	337.1	137.7	44.8	23.2	138.8	33.9	60.6
	Average	57.85	0.74	14.99	6.15	0.09	3.12	12.40	0.90	3.24	0.52	160.3	432.3	32.4	177.1	18.9	417.4	126.5	45.9	21.3	118.8	37.8	67.8
σ	2.10	0.02	0.52	0.16	0.01	0.19	2.38	0.14	0.13	0.25	13.8	80.8	1.5	17.4	2.9	41.8	8.5	1.5	1.6	20.3	5.1	7.2	

Note: Average values and standard deviations for each group are also reported.

Abbreviations: PW, painted ware; PWS, painted wares "a straccio"; SW, slipped wares.

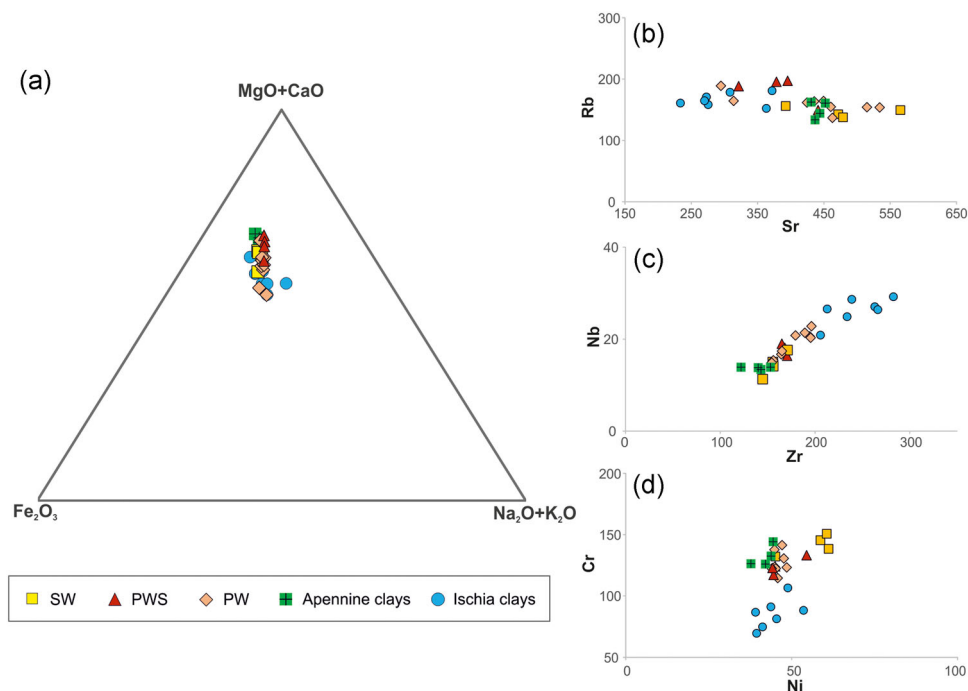


FIGURE 3 Compositional diagrams reporting the chemical composition of analysed pottery in terms of representative major (a) and trace (b–d) elements. High-CaO Apennine (samples GP1, CVR1, MCR1, and RUF 1) and Ischia clays (IS1, IS3, IS6, DA1, DA2, DA5, DA6) from De Bonis et al. (2013, 2016) were also plotted in the compositional diagrams for comparison [Color figure can be viewed at wileyonlinelibrary.com]

The mineral chemistry of volcanic phases was investigated via EDS in to determine their provenance, as they are occasionally recognized as tempering material in the analysed vessels. Feldspars are mainly K-feldspar ($An_0Ab_{7-27}Or_{73-93}$) along with lesser plagioclase ($An_{4-69}Ab_{26-91}Or_{1-5}$; Table S2 and Figure 1a). Uncolored and pale green clinopyroxene is mainly diopside or Fe-rich diopside (Morimoto, 1988), along with rare crystals of hedenbergite in volcanic scoriae of the specimen MDC 38/22 (Table S3 and Figure S1b). Some clinopyroxene crystals are zoned, with Fe-rich rims and Mg-rich cores (Table S3). Biotite crystals display variable Mg# [molar $Mg/(Mg + Fe + Mn)$] (31–54 mol.%), garnet is primarily andradite (63 mol%) (Locock, 2008), and amphibole shows a Fe-pargasitic composition (Leake et al., 2004; Table S4). Juvenile volcanics consist of scoriae, pumices and obsidians; leucite-bearing scoriae also occur in sample MDC 38/22. Hematite, Ti-oxides, and zircon (Table S4) represent other accessory phases.

However, the coexistence of such volcanic fragments with siliciclastic grains lead us to infer the use of a naturally selected deposit, likely an alluvial sand, that mixed together Apennine sandy-like materials along with volcanics from the Vesuvius environs. The provenance of volcanics from the Vesuvian districts is suggested by the occurrence of leucite-bearing scoriae and andraditic garnet, which are typical of the volcanic products of the Somma-Vesuvius activity (De Bonis et al., 2016; Guarino et al., 2016).

Only the temper observed in sample MDC 49/30 consists predominantly of siliciclastic phases scattered in the clayey matrix. Coarser grains are mainly quartz, alkali feldspar, and rounded arenaceous and silty detrital fragments (Table 3). Thus, for this sample

the use of a sand likely containing a predominantly siliciclastic component can be inferred.

The pore system was investigated by MIP and hydric tests, as porosity is useful for inferring the production technology, and depending on the types of raw materials used, the clay processing and manufacturing techniques and drying and firing conditions (Reedy, Anderson, Reedy, & Liu, 2014).

MIP and hydric tests highlighted that samples have an open and interconnected porosity ranging from 26.6% to 36.3% (Table 3). Microscopic and microstructural observations revealed that the pores are primarily subrounded or slightly elongated with a well-defined unimodal pore size distribution (Figure 5a), likely formed by trapping of air during clay processing and vessel fabrication, then enlarged with shrinkage during the firing (Reedy et al., 2014). The unimodal distribution is shown by MIP diagrams of analysed samples, characterized by similar PSD curves with a main peak of pores in a dimensional range between 0.2 and 0.4 μm and generally skewed toward finer pores (Figure 5a).

The increase of temperature during firing has effects on the pore system, resulting in the development of bigger, more rounded, and less interconnected pores (Reedy et al., 2014; Rye, 1976). However, high values of the saturation coefficient S (97–99%), as well as the small difference between free (A_b) and forced water absorption (A_f) (Table S5), attest to a general good interconnected porosity in the analyzed samples. Graphically, this behavior is expressed by the low inclination of the curve between the free and the forced adsorption (Figure 5b–d), quite flat, for example, in sample MDC 38/5 (Figure 5c). Thus, the good interconnected porosity indicates

TABLE 3 Mineralogical and textural features of ceramic pastes, determined by PLM and IA

Group samples	ID Sample	Activity of matrix	Texture	Porosity	A- plastic inclusions										GSD (mm)		Average			
					Qz	Fs	Mica	Cpx	Drf	Vgf	Cal	Hem	Grt	Amp	ϕ_{mF}	$\sigma\phi_{mF}$	C			
SW	MDC 38/17	Inactive	Bimodal	-	xxxx	xxx	-	-	tr	-	-	-	-	-	-	0.200	0.004	5.6	0.74	0.75
	MDC 38/21	Weakly Active	Seriate	33.1 ^a	xxxx	xxx	x	-	tr	tr	-	-	-	-	-	0.079	0.005	6.0	0.63	0.77
	MDC 49/4	Weakly Active	Bimodal	29.7 ^b	xxx	xxx	tr	-	xx	-	x	tr	-	-	-	0.408	0.007	5.6	0.64	0.80
	MDC 49/31	Weakly Active	Bimodal	26.8 ^a	xxxx	xxx	x	x	xx	-	-	tr	-	-	-	0.256	0.007	5.3	0.66	0.77
PWS	MDC 38/5	Weakly Active	Seriate	28.6 ^a	xxxx	xx	-	-	-	-	xx	tr	-	-	-	0.198	0.005	5.5	0.65	0.73
	MDC 38/6	Weakly Active	Seriate	31.5 ^a	xxxx	xxx	tr	-	-	tr	tr	-	-	-	-	0.186	0.008	5.2	0.66	0.75
	MDC 38/19	Weakly Active	Seriate	29.4 ^a	xxxx	xx	tr	-	-	tr	x	-	-	-	-	0.120	0.011	5.3	0.59	0.80
	MDC 39/1	Inactive	Bimodal	30.0 ^a	xxxx	xx	-	tr	tr	-	-	-	-	-	-	0.903	0.005	6.5	1.17	0.77
	MDC 38/16	Weakly Active	Bimodal	27.4 ^a	xxxx	xx	tr	tr	tr	-	-	-	-	-	-	0.253	0.003	6.7	0.73	0.78
PW	MDC 38/18	Weakly Active	Bimodal	32.7 ^b	xxxx	xxx	tr	xx	tr	x	tr	-	-	tr	-	0.364	0.004	5.4	0.82	0.76
	MDC 38/20	Weakly Active	Bimodal	30.7 ^b	xxxx	xxx	x	xx	tr	xx	tr	-	tr	-	-	0.507	0.008	5.2	0.71	0.74
	MDC 38/22	Inactive	Bimodal	27.6 ^a	xxxx	xxx	tr	xx	tr	xx	tr	-	tr	-	-	0.457	0.007	5.6	0.71	0.78
	MDC 49/29	Weakly Active	Bimodal	33.7 ^c	xxxx	xx	-	tr	tr	tr	-	-	-	-	-	0.403	0.005	5.8	0.67	0.74
	MDC 49/30	Weakly Active	Bimodal	32.5 ^c	xxxx	xxx	x	-	xx	-	-	-	-	-	-	0.412	0.006	5.7	0.85	0.77
	MDC 98/18	Weakly Active	Bimodal	28.6 ^a	xxxx	xxx	tr	tr	tr	tr	-	tr	tr	-	-	0.313	0.006	5.4	0.63	0.74
	MDC 98/19	Inactive	Bimodal	36.3 ^b	xxxx	xxx	x	x	tr	x	-	-	-	-	-	0.384	0.007	5.3	0.72	0.76
	MDC 282/48	Weakly Active	Seriate	27.5 ^a	xxxx	xx	x	-	-	-	-	xx	-	-	-	0.252	0.005	5.7	0.58	0.78

Note: Abbreviations of minerals according Whitney and Evans (2010).

Abbreviations: Amp, amphibole; Cal, calcite; Cham, chamotte; Cpx, clinopyroxene; Drf, Detrital rock fragments; Fsp, feldspar; Grn, garnet; Hem, hematite; Ol, olivine; PW, painted ware; PWS, painted wares "a straccio"; Qz, quartz; SW, slipped wares; tr, traces; Vgf, volcanic glass fragments; $\sigma\phi_{mF}$, standard deviation of ϕ_{mF} values.

^aPorosity determined by hydric tests.

^bPorosity determined by MIP.

^cAverage value of porosity obtained by MIP and hydric tests (for the results obtained by each method, see Supporting Information).

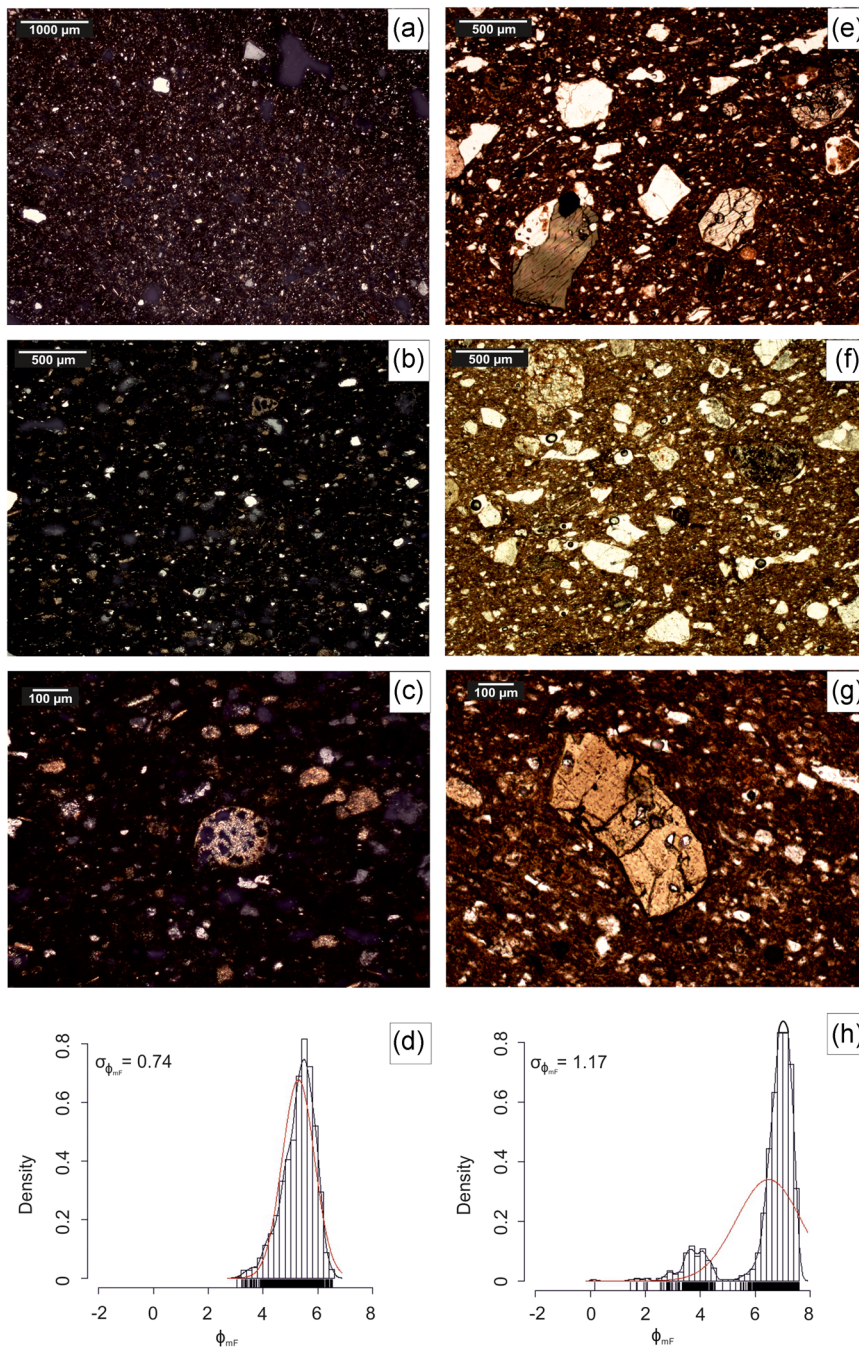


FIGURE 4 Photomicrographs of representative samples and density histograms of GSD. (a) sample MDC 38/5, ceramic body, crossed polars, $\times 20$; (b) sample MDC 38/6, ceramic body, crossed polars, $\times 40$; (c) sample MDC 38/6, fossil shell, crossed polars, $\times 200$; (d) sample MDC 38/19, GSD; (e) sample MDC 38/20, ceramic paste with volcanic temper, plane polarized light, $\times 40$; (f) sample MDC 49/30, ceramic paste with siliciclastic temper, plane polarized light, $\times 40$; (g) sample MDC 38/22, garnet crystal, plane polarized light, $\times 200$; (h) sample MDC 39/1, GSD [Color figure can be viewed at wileyonlinelibrary.com]

that firing temperatures were not high enough to produce isolated vesicles and/or bloated pores due to trapped gases as the clay matrix and silica minerals begin to melt, off-gas, and vitrify (Choo et al., 2004).

6.3 | Ceramic slips

After molding and drying, the vessels were decorated by applying a quick, rough slip; in our case, the external appearance of pottery

allowed for classification of the different categories of vessels (i.e., SW, PWS, PW).

SW pottery showed reddish (average $L^* = 49.61$; average $a^* = 24.51$; average $b^* = 27.38$) or brownish slips (average $L^* = 54.17$; average $a^* = 14.41$; average $b^* = 20.78$; Table 4) applied on both the internal and external surfaces by immersion. Coatings appeared rather well-preserved; a compact layer of ca. 15–20 μm (dashed line in Figure 6a) covered the walls showing the typical structural features of a smoothing made before the immersion in the pigment mixture (Ionescu, Hoeck, Crandell, & Šarić, 2015).

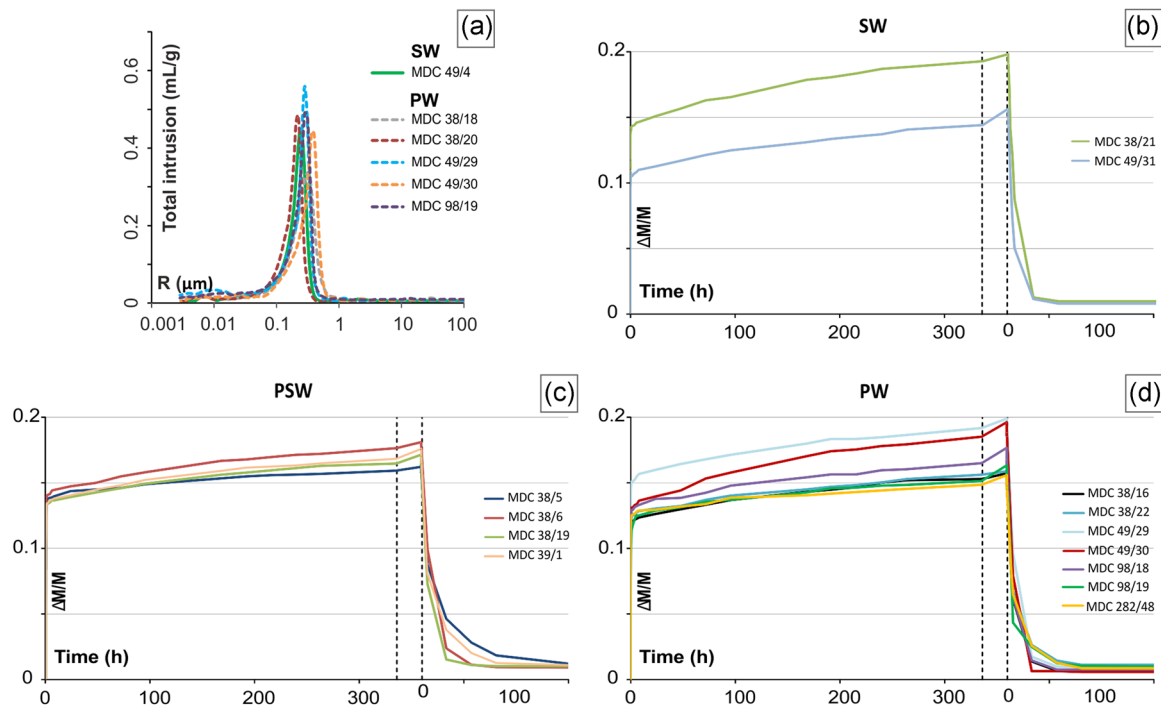


FIGURE 5 Pore-size distribution (a) and water absorption (b–d) curves of ceramic samples. PW, painted ware; PWS, painted wares “a straccio”; SW, slipped wares [Color figure can be viewed at wileyonlinelibrary.com]

Micro-Raman spectroscopy of red slips showed the typical peaks of hematite at ca. 295, 410, 500, 610 cm^{-1} (Bikiaris et al., 2000; Germinario, Izzo, et al., 2018; Mioč, Coloman, Sagon, Stojanović, & Rosić, 2004) along with silicate impurities as quartz (weak band at ca.

460 cm^{-1} ; Figure 6a). The mineralogical composition led us to infer the use of red earths (ochre) as a colorant for the surfaces.

By contrast, brown slips showed the distinctive Raman peaks of magnetite (ca. 371, 675 cm^{-1} ; Shebanova & Lazor, 2003; Figure 6a),

TABLE 4 Colorimetric features (by colorimetric analyses) and optical properties (by PLM) of ceramic slips

Ceramic class	ID sample	Optical activity (by PLM)	Color (from Munsell)	Colorimetric coordinates		
				L*(D65)	a*(D65)	b*(D65)
SW	MDC 38/17	Inactive	7.5 YR 6/4 Light brown	57.29	13.27	20.35
	MDC 38/21	Birefringent	2.5 YR 4/6 Red	48.31	23.96	24.25
	MDC 49/4	Inactive	7.5 YR 4/3 Brown	51.05	15.55	21.22
	MDC 49/31	Birefringent	5 YR 5/8 Yellowish red	50.91	25.06	30.51
PWS	MDC 38/5	Birefringent	2.5 YR 5/6 Red	51.09	22.98	26.33
	MDC 38/6	Inactive	7.5 YR 4/2 Brown	46.41	6.59	14.63
	MDC 38/19	Inactive	7.5 YR 4/3 Brown	49.04	8.62	15.15
	MDC 39/1	Birefringent	2.5 YR 5/8 Red	51.56	16.25	20.87
PW	MDC 38/16	Birefringent	7.5 YR 5/3 Brown	53.68	7.66	17.84
	MDC 38/18	Inactive	5 YR 4/2 Dark reddish gray	49.03	6.82	10.44
	MDC 38/20	Birefringent	2.5 YR 6/8 Light red	59.36	16.26	27.25
	MDC 38/22	Birefringent	5 YR 5/6 Yellowish red	56.01	17.97	25.44
	MDC 49/29	–	5 YR 3/2 Dark reddish brown	51.49	4.35	12.17
	MDC 49/30	Birefringent	10 YR 5/6 Yellowish brown	49.96	22.46	23.67
	MDC 98/18	Inactive	10 YR 3/2 Dark gray	46.71	5.27	11.57
	MDC 98/19	–	10 YR 2/1 Black	40.85	5.14	9.55
	MDC 282/48	–	2.5 YR 5/8 Red	54.68	16.98	24.87

Note: Color notations obtained from visual inspection by using Munsell Soil Color Chart were also reported.

Abbreviations: PW, painted ware; PWS, painted wares “a straccio”; SW, slipped wares.

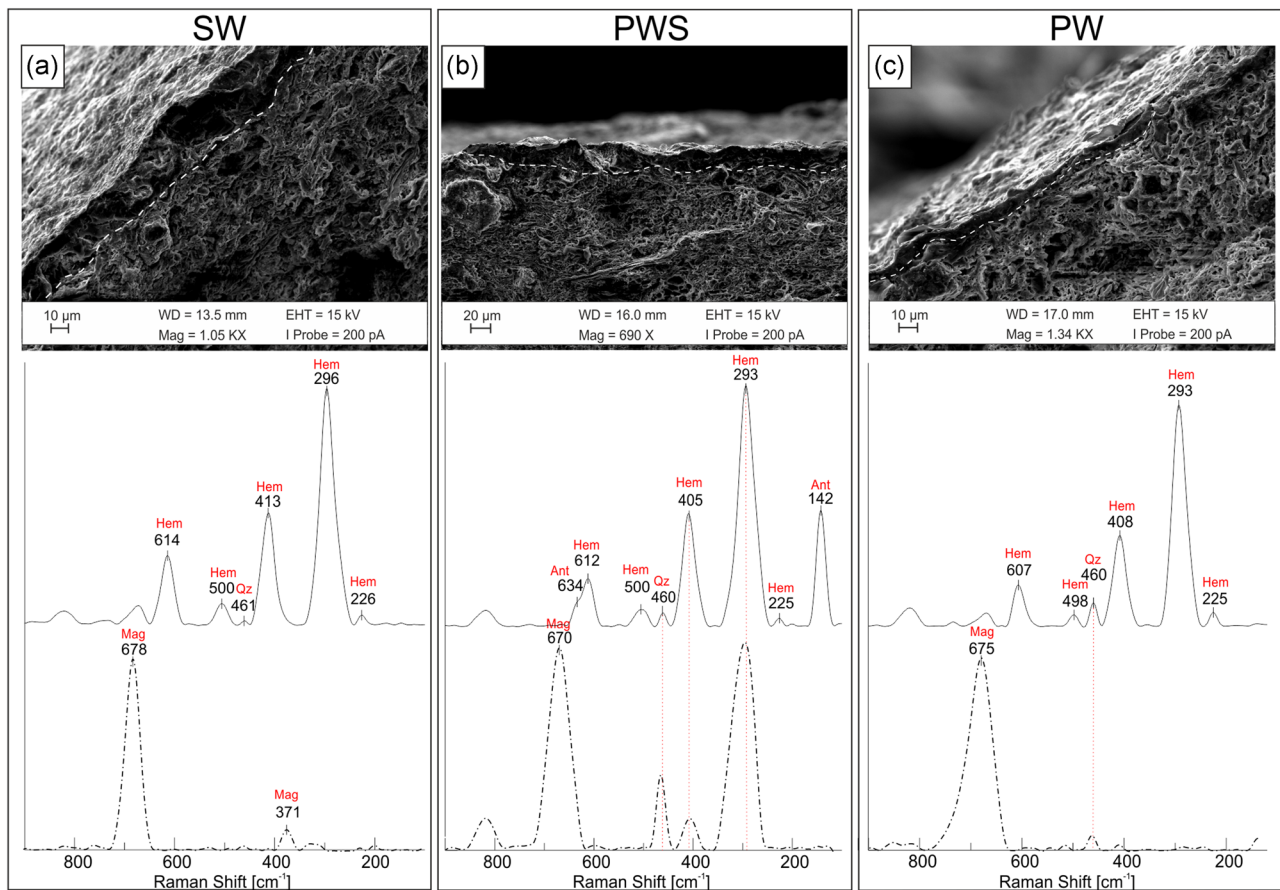


FIGURE 6 Secondary electron images of ceramic slips of SW (a), PWS (b), and PW (c) samples. Representative Raman spectra of red (solid line), brown or black slips (dotted line) of each ceramic class are also reported (abbreviation, Whitney & Evans, 2010). Ant, anatase; Hem, hematite; Mag, magnetite; Qz, quartz [Color figure can be viewed at wileyonlinelibrary.com]

suggesting a firing step characterized by a reducing atmosphere to obtain the darker color of slips from the same red earth starting material (Germinario, Cultrone, et al., 2018).

PWS also showed slip coatings of red (average $L^* = 50.06$; average $a^* = 15.80$; average $b^* = 20.74$) or brown (average $L^* = 47.73$; average $a^* = 7.61$; average $b^* = 14.89$) with a thickness of ca. 15–20 μm (Table 4). The slips appeared less compact and more irregular than the SW (Figure 6b), denoting a lower accuracy in the decoration as well as a rougher application technique. Nonetheless, the mineralogical composition is the same of SW. Both red and brown coatings, in fact, showed the Raman peaks of iron oxides (hematite and magnetite) and quartz (Figure 6b). Moreover, less intense bands at ca. 145 and 634 cm^{-1} were also visible (Figure 6b); they can be likely attributed to anatase (Germinario, Cultrone, et al., 2018; Sendova, Zhelyaskov, Scalera, & Ramsey, 2005), a Ti-oxide occurring as an accessory phase.

Finally, PW pottery was covered with red (average $L^* = 56.68$; average $a^* = 17.07$; average $b^* = 25.85$) or brown/black patterns (average $L^* = 48.62$; average $a^* = 8.62$; average $b^* = 14.21$) slips (Table 4 and Figure 6c).

The thickness of decoration was ca. 5 μm (Figure 6c) and Raman analyses again highlight the use of ochre, which changed hue from

red to black as a result of changing the kiln atmosphere during firing. Hematite and quartz characterized red coatings whereas magnetite was observed in the black ones (Figure 6c).

For each ceramic class, micro-textural and micro-chemical analyses confirmed spectroscopic data; SEM-EDS analyses, in fact, revealed that the slips are composed of a Si-, Al-, K-rich clay matrix in which bright Fe- and Ti-rich particles are scattered (Figure S2), consistently with the composition of the ochre pigment.

6.4 | Firing technology

The most important and critical step of ceramic production is the firing process; here, molded and decorated clay turns to pottery. Firing parameters definitely affect the color and the technical performance of pottery, and are intimately connected to the mineralogical composition in the finished pot (Molera, Pradell, & Vendrell-Saz, 1998; Valanciene, Siauciuinas, & Baltusnikaite, 2010).

The analyzed tableware is generally characterized by reddish and brownish ceramic bodies (Table 5). Colorimetric measurements highlight the occurrence of brownish samples (MDC 38/6, 38/17, 38/18, 38/19, 49/29) showing a higher average luminosity value ($L^*_{\text{avg.}} =$

TABLE 5 Colorimetric coordinates (CIE L* a* b*, illuminant C) and colors of SW, PWS, and PW samples measured via portable colorimetry

Ceramic Class	ID Sample	Zoning	Colour											
			Core						Rim			Core	Rim	
			L*	a*	b*	L*	a*	b*	L*	a*	b*			
SW	MDC 38/17	Faint	50.57	4.74	13.88	-	-	-	-	-	-			
	MDC 38/21	-	63.98	15.83	22.57	-	-	-	-	-	-			
	MDC 49/4	Faint	51.70	21.21	28.07	-	-	-	-	-	-			
	MDC 49/31	-	51.63	24.64	29.79	-	-	-	-	-	-			
PWS	MDC 38/5	Faint	-	-	-	65.46	7.81	19.52	49.58	20.69	27.49			
	MDC 38/6	-	62.60	9.94	22.20	-	-	-	-	-	-			
	MDC 38/19	-	67.27	8.34	18.38	-	-	-	-	-	-			
	MDC 39/1	Faint	-	-	-	58.77	11.17	19.10	62.93	13.53	22.73			
PW	MDC 38/16	Faint	-	-	-	48.69	3.86	9.20	56.66	8.26	16.92			
	MDC 38/18	-	58.40	13.51	24.35	-	-	-	-	-	-			
	MDC 38/20	-	55.56	16.80	27.65	-	-	-	-	-	-			
	MDC 38/22	-	60.98	14.82	24.49	-	-	-	-	-	-			
	MDC 49/29	-	62.48	6.70	15.07	-	-	-	-	-	-			
	MDC 49/30	-	56.63	19.45	25.23	-	-	-	-	-	-			
	MDC 98/18	Sharp	60.25	5.46	12.53	-	-	-	-	-	-			
	MDC 98/19	Faint	62.20	4.13	10.48	-	-	-	-	-	-			
	MDC 282/48	Sharp	-	-	-	60.43	1.40	7.25	59.82	13.74	25.74			

Note: For interpretation of the references to color in this figure, the reader is referred to the web version of this article.

60.26) and lower values of colorimetric coordinates (a^* avg. = 8.65; b^* avg. = 18.77), whereas a lower average luminosity value (L^* avg. = 56.75) and higher average values of a^* (a^* avg. = 18.79) and b^* (b^* avg. = 26.30) distinguish reddish specimens (MDC 38/20, 38/21, 38/22, 49/4, 49/30, 49/31) (Table 5). It is worth noting that some samples (MDC 38/5, 38/16, 39/1, 282/48) showed a color zoning of ceramic bodies.

This sandwich-like structure is also present in the samples MDC 38/17, 49/29, 98/18, 98/19, where a darker core, likely due to an incomplete oxidation of the inner ceramic body, was observed (De Bonis et al., 2017; Maritan, Nodari, Mazzoli, Milano, & Russo, 2006; Nodari, Maritan, Mazzoli, & Russo, 2004). However, colorimetric analyses did not allow measuring each portion due to the large spot size (ca. 3 mm; Table 5).

The color is a striking feature of ceramics and depends on the chemical and mineralogical composition of the clayey raw materials used, the temperatures and redox conditions achieved during firing (De Bonis et al., 2017). The use of HCC raw materials of the same origin and the presence of mineralogical phases indicating oxidizing conditions (see later), led us to infer that color was only affected by the firing process experienced by vessels, which can be evaluated by estimating the equivalent firing temperatures (hereafter EFT). To this end, microstructural (SEM) and quantitative mineralogical (XRPD) analyses were performed.

SEM observations showed microstructural features typical of an extensive vitrification stage (V) (Maniatis & Tite, 1981). The firing developed a dense network of melted clay particles connected together, in some cases limiting rounded and/or elongated pores (Figure 7a,b). In high-CaO samples, this vitrification structure remains essentially unchanged in the thermal range between 850°C

and 1,050°C (Maniatis & Tite, 1981), consistent with the mineralogical assemblage observed by XRPD and with the porosity analyses (De Bonis et al., 2014). Actually, mineralogical analyses reflect both residual minerals from the original clayey material and newly formed phases generally developing at temperatures of 850°C or higher (Table 6). Quartz and feldspars constitute the most abundant phases (Table 6). Calcite was also detected as well as hematite that consistently varies from 1 to 2 wt% (Table 6). The latter suggests an oxidizing environment during firing (Nodari, Maritan, Mazzoli, & Russo, 2007). Moreover, traces of residual (10 Å) illite-like phases were observed (Table 6).

The firing process experienced by this Ca-rich pottery resulted in the nucleation of newly formed Ca-silicates (e.g., gehlenite and/or Ca-rich pyroxene), representing distinctive thermal markers for the EFT estimation. Their formation is due to the interaction between decomposed Ca- (and/or Mg-) carbonates and Si- and Al-rich material deriving from the breakdown of clay minerals (Cultrone, Rodriguez-Navarro, Sebastián, Cazalla, & De La Torre, 2001). As highlighted by SEM-EDS analyses, newly formed Ca-silicates developed at the interface between decomposed carbonate grains and the clayey matrix, forming a reaction rim with the composition of gehlenite (Figure 7c) and/or Ca-Al-rich pyroxene (Figure 7d). These phases were detected in variable amounts by quantitative XRPD in the analysed vessels. Ca-rich pyroxene varies from 5% to 13% whereas melilite occurs in lower amounts (1–6%; Table 6). Although these newly formed phases nucleated at the expenses of carbonates and clay minerals, calcite was detected along with gehlenite, often in similar amounts (Table 6). It is widely accepted that the increase of temperature in the kiln results in the decomposition of carbonate

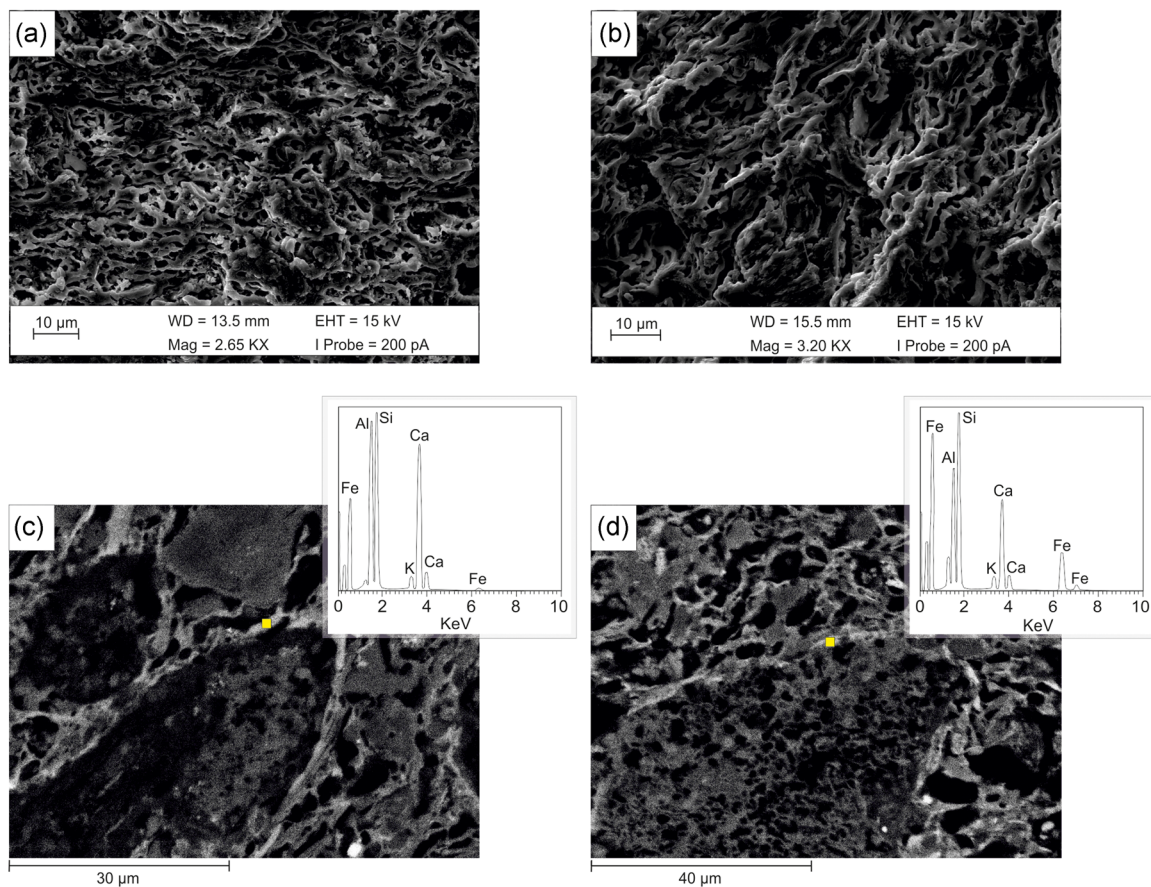


FIGURE 7 (a) Microtextures of sample MDC 49/4 (secondary electrons images), representative of an extensive vitrification stage (V); (b) sintering structure of sample MDC 49/30; (c,d) SEM images in BSEs of sample MDC 38/6 (c) and MDC 38/18 (d) showing the reaction rims around calcite crystals showing the typical chemical composition of newly formed gehlenite and Ca-rich clinopyroxene, respectively (EDS spectra are referred to the yellow spots in the images). BSE, backscattered electron; EDS, energy-dispersive X-ray spectroscopy; SEM, scanning electron microscopy [Color figure can be viewed at wileyonlinelibrary.com]

favoring the formation of Ca-silicates (Dondi, Ercolani, Fabbri, & Marsigli, 1998; Rathossi & Pontikes, 2010). Thus, in samples where Ca-silicates occurred along with calcite crystals still visible in ceramic bodies (MDC 38/5, MDC 282/48), the firing temperatures and/or soaking time were not sufficient for complete decomposition of calcite.

By contrast, in other samples in which only calcite was detected via XRPD (and not by PLM; Table 3), the origin of the phase should be considered as a secondary product, either (a) derived from the crystallization from free-lime produced by the thermal decomposition of initial calcite; (b) precipitated from carbonate-rich solutions that filtered into the ceramics during burial; or (c) formed by alteration of gehlenite in the ceramic material during the burial (Fabbri, Gualtieri, & Shoal, 2014). As a matter of fact, gehlenite is a metastable phase that forms different reaction products during burial depending on the composition of soil solutions and can turn to calcite plus smectite (Grifa et al., 2018; Heimann, 2017).

Thus, because gehlenite may also form during postburial alteration (and not just during firing), its use in estimating firing temperatures could be misleading (Figure 8a). Perhaps a more useful thermal marker is the amount of newly formed Ca-pyroxene.

In particular, EFTs can be more properly inferred if one takes into account the amount of newly formed Ca-pyroxene and considers its correlation with the amount of LO-AP (Figure 8b). This relationship could depend on higher firing temperatures that favor the formation of stable crystalline phases (e.g., Ca-pyroxene) at the expense of partially or completely disordered phases derived from the dehydroxylation of clay-minerals.

It is also interesting to note the close relationship between mineralogical composition (in particular Ca-rich pyroxene content) and the color of ceramic bodies. In particular, clusters of reddish and brownish samples observed on the basis of colorimetric measurements broadly reflect different mineralogical assemblages.

As shown in the diagrams in Figure 8c,d that plot colorimetric coordinates values against the amount Ca-pyroxene, samples with bright reddish ceramic bodies are characterized by a content of Ca-pyroxene lower than 9%, whereas samples with brownish matrices have higher content of Ca-rich pyroxene (>9%).

This behavior is in a quite good agreement with experimental results obtained on ceramic replicas by De Bonis et al. (2017), who recognized a decrease in color saturation (b^* values) from 900°C. This is normally related to the development of newly formed

TABLE 6 Quantitative XRPD data and estimated EFTs

Ceramic Class	ID sample	Quartz	Feldspar	Illite/mica	Calcite	Clinopyroxene	Gehlenite	Hematite	LO-AP	EFT
SW	MDC 38/17	22	25	–	6	5	4	1	37	850–900°C
	MDC 38/21	21	27	tr	4	10	5	1	32	900–950°C
	MDC 49/4	19	23	tr	6	9	5	2	36	900–950°C
	MDC 49/31	19	17	tr	6	6	5	1	46	850–900°C
PWS	MDC 38/5	20	11	tr	9	5	2	1	52	800–850°C
	MDC 38/6	20	21	tr	7	10	6	1	35	900–950°C
	MDC 38/19	17	22	tr	3	12	6	1	39	900–950°C
	MDC 39/1	25	23	tr	5	8	2	1	36	850–900°C
PW	MDC 38/16	26	24	tr	2	8	3	1	36	850–900°C
	MDC 38/18	21	28	tr	3	11	4	1	32	900–950°C
	MDC 38/20	19	23	tr	3	11	4	1	39	900–950°C
	MDC 38/22	19	22	tr	6	12	3	1	37	900–950°C
	MDC 49/29	19	31	tr	2	12	4	1	31	900–950°C
	MDC 49/30	28	27	tr	1	6	1	2	35	850–900°C
	MDC 98/18	15	32	tr	2	13	2	1	35	900–950°C
	MDC 98/19	17	40	tr	2	13	3	1	24	900–950°C
MDC 282/48	19	16	tr	9	5	1	–	50	800–850°C	

Abbreviations: EFT, equivalent firing temperature; PW, painted ware; PWS, painted wares “a straccio”; SW, slipped wares; XRPD, X-ray powder diffraction.

Ca-silicates (e.g., pyroxene, melilite), which incorporate the iron in their structure hindering its transformation into hematite (e.g., Molera et al., 1998). Therefore, according to the experimental data, we can likely suppose that samples showing brownish hues and higher amounts of Ca-pyroxene experienced higher firing temperatures (>900°C) with respect to the reddish samples that were reasonably fired at lower temperatures (800–900°C; Table 6).

Thus, it appears evident that the resulting mineral assemblages and color of ceramic bodies strictly depend on the firing temperatures experienced by the vessels. Furthermore, firing regimes produced textural and physical changes that also influenced the porosity as indicated by the correlations of porosity measurements with the mineralogical and colorimetric data. Actually, the porosity of analysed vessels tends to increase with the newly formed clinopyroxene content (viz., with the increase of EFT; Figure 8e). Likewise, a decrease in the apparent density values ρ_b is evident (Figure 8f). This behavior is connected with textural changes occurring in the ceramic bodies during the firing; in fact, the increase in firing temperatures results in the formation of larger pores and, in HCC, the development of microcracking generated by the decomposition of carbonates (i.e., “lime blowing”) also leads to a general increase in porosity and pore volume, which results in the increase in open porosity and the decrease in the apparent density ρ_b values (Cultrone et al., 2004; De Bonis et al., 2014; Grifa et al., 2009).

7 | CONCLUSIONS

Archaeometric analyses performed on the samples collected in the archaeological site of Pollena Trocchia provide information on the pottery circulating in the northern Vesuvius area during the late

Roman period. In this period, the Vesuvius' hinterland was characterized by the presence of local workshops scattered in the countryside (Arthur, 2007) that resulted in a predominance of local pottery with respect to imported African productions that could be explained in terms of the relative penetration of the imported goods. The local productions did not fulfill the self-sufficiency of the market, favouring the development of a dense network of micro-regional commercial trade routes along with importation to guarantee the availability of vessels with different functions (Carsana, D'Amico, & Del Vecchio, 2007; Martucci et al., 2014; Toniolo, 2012).

In the first stage, local late Roman common wares only integrated the markets provided by ARS, and acquired their own typological identity. The change in the shape repertoire was also reflected in the application of the colored slips, moving from immersion likely in a mixture of water and earth pigments (i.e., SW) to the rough application of the color with a cloth or a brush on the external surfaces and rims (i.e., PWS). The production of new (and bigger) shapes, in fact, required a new technique for coloring the surface of the vases using a paint brush or a cloth (the “straccio”) dipped in the color, a less complicated and less expensive method than immersion. Then, PW provided a further change in the decoration, evolved in the creation of rudimentary, striped decorative patterns on the external surfaces.

Nonetheless, this archaeometric study illustrates that the morphological and decorative changes did not involve any changes in the raw materials used or the firing technology adopted for their production. Actually, specific geomaterials had been exploited over the entire time span studied. Due to their outstanding suitability for ceramics production, in fact, Miocene-Pleistocene clay deposits in Campania along the Apennine chain (i.e., Salerno, Montesarchio, Calvi Risorta) were used at the Pollena site, as well as for other pottery

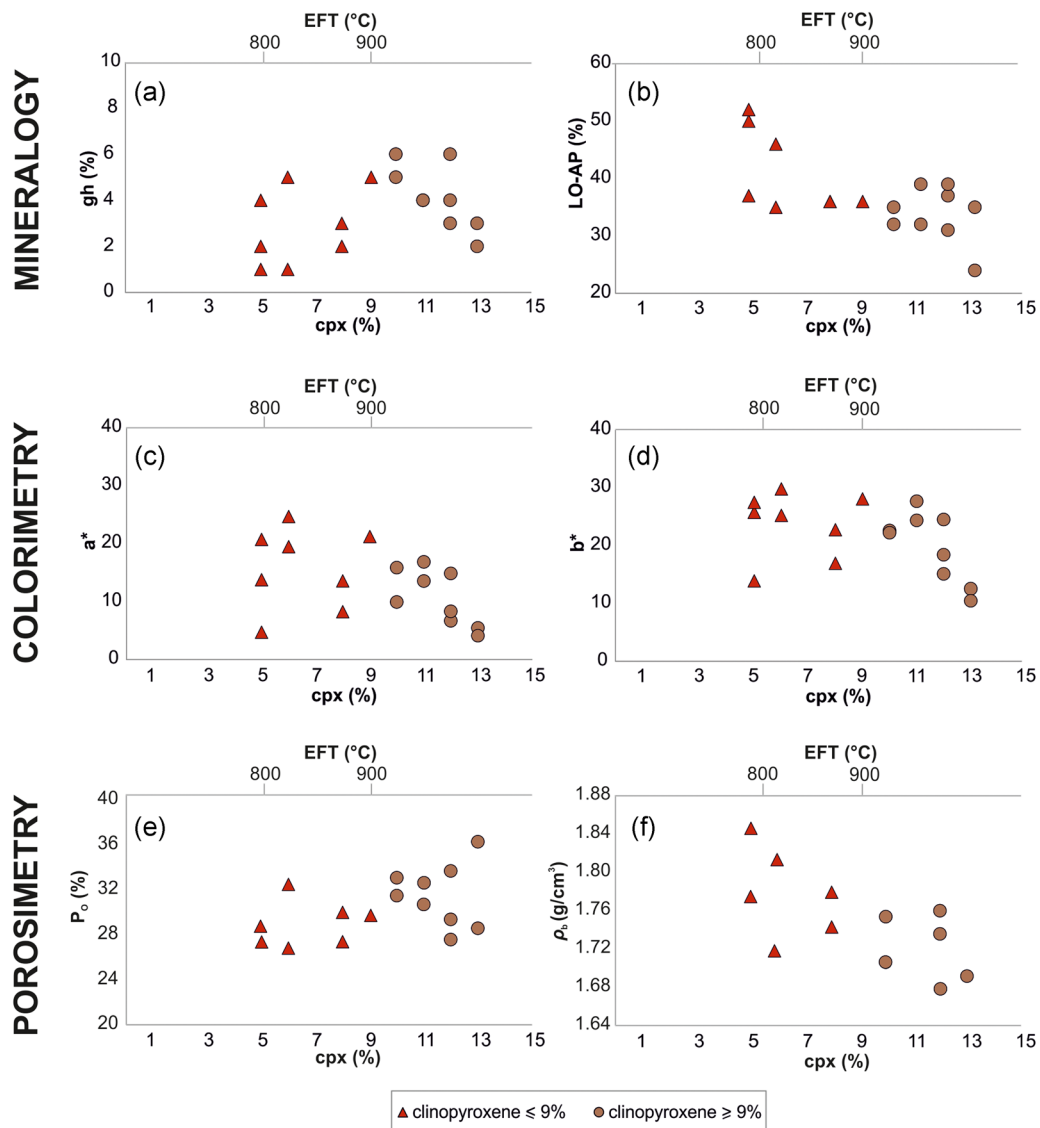


FIGURE 8 Binary diagrams comparing the content of Ca-pyroxene with mineralogical data, colorimetric coordinates, and porosimetric parameters of the analysed samples. (a) Clinopyroxene versus gehlenite contents diagram; (b) clinopyroxene versus LO-AP contents diagram that shows their inverse relationship; (c) clinopyroxene content versus values of the colorimetric coordinate a^* ; (d) clinopyroxene content versus values of the colorimetric coordinate b^* ; (e) open porosity and (f) apparent density versus clinopyroxene content diagrams [Color figure can be viewed at wileyonlinelibrary.com]

productions in the Bay of Naples (De Bonis et al., 2010, 2013; Grifa et al., 2009, 2019; Peña & McCallum, 2009a; Scarpelli et al., 2014). Moreover, it is observed that a local sandy-silty material was occasionally used as temper, consisting of naturally mixed deposits containing siliciclastic and volcanic phases, the latter showing a mineral chemistry consistent with Somma-Vesuvius rocks. The exploitation of the Miocene-Pleistocene clay deposits inferred that despite the profound changes in this area due to political events and geologic disasters (earthquakes and volcanic eruptions), the commercial relationships in providing raw materials were still actively maintained.

Firing was performed in a quite narrow range of temperatures (800–950°C), as suggested by mineralogy (e.g., the occurrence of Ca-silicates) and microstructure (pervasive sintering of ceramic bodies). The different shades of reddish and brownish colors of the ceramic

bodies can be attributed to slightly different firing temperatures. As a matter of fact, the increase in Ca-rich pyroxenes at higher firing temperatures gave rise to more brown ceramic bodies. Moreover, the presence of hematite suggests a firing process in oxidizing conditions, although observed color zoning in some ceramic bodies reflects a low accuracy in the technological process and/or a shorter firing duration, likely insufficient to completely reoxidize the whole ceramic body, resulting in a darkening of cores (De Bonis et al., 2017). However, the presence of organic matter in the clay paste, which may result in reduction and cause a black core (Maritan et al., 2006), should also be taken into account.

However, the discriminating technological feature among the different types of these color coated tablewares is in the modality of application of decoration, made with an earth-based pigment, as

determined by μ -Raman spectroscopy. The decorative technique changed over time, passing from the abandonment of high-quality vessels decorated with compact and/or sintered slips to the application of the coating by immersion in a sort of semi-liquid iron-rich clay suspension (i.e., SW), to a new decorative technique with a cloth/sponge (i.e., PWS) or with a brush (i.e., PW).

As stated by Martucci and coauthors (Martucci et al., 2018), this change in the decorative technique is probably related to a technological adaptation. The transition from SW to PWS likely responded to the need for a cheaper and faster decoration of larger open shapes characterizing the PWS, whereas the transition to PW decorated with a brush is due to a desire to create elementary, decorative patterns.

Such a technological change reflects the late Roman political and socioeconomic context; the expansion of smaller rural production centers covering new market needs, in fact, determined the development of self-sufficient and functional productions at the expense of the aesthetical features of vessels.

ACKNOWLEDGMENTS

This study was supported by grants from the *Dipartimento di Scienze e Tecnologie* of the *Università degli Studi del Sannio* (FRA 2015 CG) and by the research group RNM179 of the Junta de Andalucía and research project MAT2016-75889-R. The authors kindly thank Prof. Piergiulio Cappelletti for XRPD patterns acquisition. The authors also kindly thank two anonymous reviewers that definitively helped to improve the manuscript.

ORCID

Chiara Germinario  <http://orcid.org/0000-0003-0912-0503>
 Giuseppe Cultrone  <http://orcid.org/0000-0001-9503-3312>
 Alberto De Bonis  <http://orcid.org/0000-0002-8088-9481>
 Girolamo F. De Simone  <http://orcid.org/0000-0003-4489-7385>
 Francesco Izzo  <http://orcid.org/0000-0002-4639-1241>
 Alessio Langella  <http://orcid.org/0000-0003-3029-2713>
 Mariano Mercurio  <https://orcid.org/0000-0003-3469-5907>
 Vincenzo Morra  <http://orcid.org/0000-0002-3310-8603>
 Christopher R. Vyhna  <https://orcid.org/0000-0002-0184-8754>
 Celestino Grifa  <http://orcid.org/0000-0003-4723-8158>

REFERENCES

- Arrighi, S., Principe, C., & Rosi, M. (2001). Violent strombolian and subplinian eruptions at Vesuvius during post-1631 activity. *Bulletin of Volcanology*, 63, 126–150.
- Arthur, P. (1987). Produzione ceramica e agro Falerno. In G. Guadagno (Ed.), *Storia, economia ed architettura nell'ager Falernus* (pp. 59–68). Minturno, Italy: Caramanica Editore.
- Arthur, P. (2007). Form, function and technology in pottery production from late antiquity to early middle ages. In L. Lavan, E. Zanini & A. Sarantis (Eds.), *Late antiquity archaeology* (Vol. 4, pp. 159–184). Boston, MA: Brill, Leiden.
- Arthur, P., & Soricelli, G. (2015). Produzione e circolazione della ceramica tra Campania settentrionale e area vesuviana in età tardoantica (IV–VI secolo). In N. Busino & M. Rotili (Eds.), *Inseguimenti e Cultura Materiale Fra Tarda Antichità e Medioevo* (pp. 141–157). San Vito al Tagliamento, Italy: Tavolario Edizioni.
- Barberi, F., Davis, M. S., Isaia, R., Nave, R., & Ricci, T. (2008). Volcanic risk perception in the Vesuvius population. *Journal of Volcanology and Geothermal Research*, 172, 244–258.
- Barilaro, D., Barone, G., Crupi, V., Donato, M. G., Majolino, D., Messina, G., & Ponterio, R. (2005). Spectroscopic techniques applied to the characterization of decorated potteries from Caltagirone (Sicily, Italy). *Journal of Molecular Structure*, 744–747, 827–831.
- Bikiaris, D., Daniilia, S., Sotiropoulou, S., Katsimbiri, O., Pavlidou, E., Moutsatsou, A. P., & Chrysosoulakis, Y. (2000). Ochré-differentiation through micro-Raman and micro-FTIR spectroscopies: Application on wall paintings at Meteora and Mount Athos, Greece. *Spectrochimica Acta—Part A: Molecular and Biomolecular Spectroscopy*, 56, 3–18.
- Bish, D. L., & Reynolds, R. C. J. (1989). Modern powder diffraction. In D. L. Bish & J. E. Post (Eds.), *Reviews in mineralogy* (20, pp. 73–99). Chantilly, VA: Mineralogical Society of America.
- Bonifay, M. (2014). Céramique africaine et imitations: Où, quand, pourquoi? In R. Morais, A. Fernández & M. J. Sousa (Eds.), *As produções cerâmicas de imitação na Hispania* (pp. 75–91). Porto: Monografias Ex Officina Hispana II.
- Bowersock, G. W., Brown, P., & Grabar, O. (1999). *Late antiquity: A guide to the postclassical world*. Cambridge, MA: Belknap Press.
- Carsana, V., D'Amico, V., & Del Vecchio, F. (2007). Nuovi dati ceramologici per la storia economica di Napoli tra tarda antichità ed altomedioevo. In M. Bonifay & J.-C. Treglia (Eds.), *LRCW 2, Late roman coarse wares, Cooking wares and amphorae in the Mediterranean. Archaeology and archaeometry* (Vol. 1, pp. 423–437). Oxford: Bar International Series 1662 I, Archaeopress.
- Choo, C. K. K., Lee, Y. E., Shim, I. W., Kim, G. H., Huh, W. Y., Chun, S. C., & Choo, W. K. (2004). Compositional and Microstructural Study of Koryŏ Celadon and Whiteware Excavated from SŌri Kiln in Kyŏnggi Province. *Archaeometry*, 46, 247–265.
- Cioni, R., Santacroce, R., & Sbrana, A. (1999). Pyroclastic deposits as a guide for reconstructing the multi-stage evolution of the Somma-Vesuvius Caldera. *Bulletin of Volcanology*, 61, 207–222.
- Coticelli, S., Laurenzi, M. A., Giordano, G., Mattei, M., Avanzinelli, R., Melluso, L., ... Perini, G. (2010). Leucite-bearing (kamafugitic/leucitic) and -free (lamproitic) ultrapotassic rocks and associated shoshonites from Italy: Constraints on petrogenesis and geodynamics. *Journal of the Virtual Explorer*, 36(20), 1–95.
- Cultrone, G., Molina, E., & Arizzi, A. (2014). The combined use of petrographic, chemical and physical techniques to define the technological features of Iberian ceramics from the Canto Tortoso area (Granada, Spain). *Ceramics International*, 40, 10803–10816.
- Cultrone, G., Rodríguez-Navarro, C., Sebastián, E., Cazalla, O., & De La Torre, M. J. (2001). Carbonate and silicate phase reactions during ceramic firing. *European Journal of Mineralogy*, 13, 621–634.
- Cultrone, G., Sebastián, E., Elert, K., de la Torre, M. J., Cazalla, O., & Rodríguez-Navarro, C. (2004). Influence of mineralogy and firing temperature on the porosity of bricks. *Journal of the European Ceramic Society*, 24, 547–564.
- De Bonis, A., Arlenzo, I., D'Antonio, M., Franciosi, L., Germinario, C., Grifa, C., ... Morra, V. (2018). Sr-Nd isotopic fingerprinting as a tool for ceramic provenance: Its application on raw materials, ceramic replicas and ancient pottery. *Journal of Archaeological Science*, 94, 51–59.
- De Bonis, A., Cultrone, G., Grifa, C., Langella, A., Leone, A. P., Mercurio, M., & Morra, V. (2017). Different shades of red: The complexity of mineralogical and physico-chemical factors influencing the colour of ceramics. *Ceramics International*, 43, 8065–8074.
- De Bonis, A., Cultrone, G., Grifa, C., Langella, A., & Morra, V. (2014). Clays from the Bay of Naples (Italy): New insight on ancient and traditional ceramics. *Journal of the European Ceramic Society*, 34, 3229–3244.
- De Bonis, A., Febbraro, S., Germinario, C., Giampaola, D., Grifa, C., Guarino, V., ... Morra, V. (2016). Distinctive volcanic material for the production of campana A ware: The workshop area of Neapolis at the Duomo metro station in Naples, Italy. *Geoarchaeology*, 31, 437–466.

- De Bonis, A., Grifa, C., Cultrone, G., De Vita, P., Langella, A., & Morra, V. (2013). Raw materials for archaeological pottery from the Campania region of Italy: A petrophysical characterization. *Geoarchaeology*, 28, 478–503.
- De Bonis, A., Grifa, C., Langella, A., Mercurio, M., Perrone, M. L., & Morra, V. (2010). Archaeometric study of roman pottery from Caudium area (Southern Italy). *Periodico di Mineralogia*, 79, 73–89.
- De Simone, G. F., Castaldo, V., & Sannino, S. (2018). Four pottery assemblages buried by Late Antique eruptions of Vesuvius. *Rei Cretariae Romanae Fautores Acta*, 45, 299–309.
- De Simone, G. F., & Macfarlane, R. T. (2009). *Apolline project vol.1: Studies on Vesuvius' north slope and the Bay of Naples*. Napoli: Università Suor Orsola Benincasa—Brigham Young University.
- De Simone, G. F., Martucci, C. S., Grifa, C., De Bonis, A., Guarino, V., & Morra, V. (2012). Late antique connectivity: A snapshot of regional trade in AD 472 Campania. In L. Bombardieri, A. D'Agostino, G. Garducci, V. Orsi & S. Valentini (Eds.), *SOMA 2012. Identity and connectivity* (2, pp. 971–980). Oxford: BAR International Series 2581 II, Archeopress.
- Dondi, M., Ercolani, G., Fabbri, B., & Marsigli, M. (1998). An approach to the chemistry of pyroxenes formed during the firing of Ca-rich silicate ceramics. *Clay Minerals*, 33, 443–452.
- Fabbri, B., Gualtieri, S., & Shoval, S. (2014). The presence of calcite in archeological ceramics. *Journal of the European Ceramic Society*, 34, 1899–1911.
- Fontana, S. (1998). Le "imitazioni" della sigillata africana e le ceramiche da mensa italiane tardo-antiche. In L. Sagui (Ed.), *La Ceramica in Italia: VI-VII secolo: atti del convegno in onore di John W. Hayes: Roma, 11-13 maggio 1995* (pp. 83–100). Firenze: All'insegna del Giglio.
- Forni, F., Degruyter, W., Bachmann, O., De Astis, G., & Mollo, S. (2018). Long-term magmatic evolution reveals the beginning of a new caldera cycle at Campi Flegrei. *Science Advances*, 4(11), eaat9401.
- Germinario, C., Cultrone, G., De Bonis, A., Izzo, F., Langella, A., Mercurio, M., ... Grifa, C. (2018). The combined use of spectroscopic techniques for the characterisation of Late Roman common wares from Benevento (Italy). *Measurement*, 114, 515–525.
- Germinario, C., Cultrone, G., Cavassa, L., De Bonis, A., Izzo, F., Langella, A., ... Grifa, C. (2019). Local production and imitations of Late Roman pottery from a well in the Roman necropolis of Cuma in Naples, Italy. *Geoarchaeology*, 34, 62–79.
- Germinario, C., Grifa, C., & Di Maggio, R. M. (2019). Analisi d'immagine. In M. Mercurio, A. Langella, R. M. Di Maggio & P. Cappelletti (Eds.), *Analisi Mineralogiche in ambito Forense* (pp. 429–452). Canterano, Rome: Aracne Editrice.
- Germinario, C., Izzo, F., Mercurio, M., Langella, A., Sali, D., Kakoulli, I., ... Grifa, C. (2018). Multi-analytical and non-invasive characterization of the polychromy of important archaeological wall paintings at the Domus of Octavius Quartio in Pompeii. *European Physical Journal Plus*, 133, 359.
- Grifa, C., De Bonis, A., Langella, A., Mercurio, M., Soricelli, G., & Morra, V. (2013). A late Roman ceramic production from Pompeii. *Journal of Archaeological Science*, 40, 810–826.
- Grifa, C., Cultrone, G., Langella, A., Mercurio, M., De Bonis, A., Sebastián, E., & Morra, V. (2009). Ceramic replicas of archaeological artefacts in Benevento area (Italy): Petrophysical changes induced by different proportions of clays and temper. *Applied Clay Science*, 46, 231–240.
- Grifa, C., Germinario, C., De Bonis, A., Langella, A., Mercurio, M., Izzo, F., ... Soricelli, G. (2019). Comparing ceramic technologies: The production of Terra Sigillata in Puteoli and in the Bay of Naples. *Journal of Archaeological Science: Reports*, 23, 291–303.
- Grifa, C., Germinario, C., De Bonis, A., Mercurio, M., Izzo, F., Pepe, F., ... Langella, A. (2017). Traditional brick productions in Madagascar: From raw material processing to firing technology. *Applied Clay Science*, 150, 252–266.
- Grifa, C., Mercurio, M., Germinario, C., Bish, D. L., De Bonis, A., Cappelletti, P., ... Langella, A. (2018). Using X-ray fluorescence and diffraction to elucidate source materials and firing conditions of pompeian ceramics. *Spectroscopy*, 33, 26–30.
- Guarino, V., De Bonis, A., Faga, I., Giampaola, D., Grifa, C., Langella, A., ... Morra, V. (2016). Production and circulation of thin walled pottery from the Roman port of Neapolis, Campania (Italy). *Periodico di Mineralogia*, 85, 95–114.
- Heimann, R. B. (2017). Mineralogical and chemical alteration. In A. Hunt (Ed.), *The Oxford handbook of archaeological ceramic analysis* (pp. 1–28). Oxford: Oxford University Press.
- Inorganic Crystal Structure Database. (2014). FIZ Karlsruhe, Germany and NIST, US, PC Version 2014/1.
- Ionescu, C., Hoek, V., Crandell, O. N., & Šarić, K. (2015). Burnishing versus smoothing in ceramic surface finishing: A SEM Study. *Archaeometry*, 57, 18–26.
- Izzo, F., Grifa, C., Germinario, C., Mercurio, M., De Bonis, A., Tomay, L., & Langella, A. (2018). Production technology of mortar-based building materials from the Arch of Trajan and the Roman Theatre in Benevento, Italy. *European Physical Journal Plus*, 133, 363.
- Leake, B. E., Woolley, A. R., Birch, W. D., Burke, E. A. J., Ferraris, G., Grice, J. D., ... Whittaker, E. J. W. (2004). Nomenclature of amphiboles: Additions and revisions to the international mineralogical association's amphibole nomenclature. *American Mineralogist*, 89, 883–887.
- Locock, A. J. (2008). An Excel spreadsheet to recast analyses of garnet into end-member components, and a synopsis of the crystal chemistry of natural silicate garnets. *Computers & Geosciences*, 34, 1769–1780.
- Mackensen, M., & Schneider, G. (2002). Production centres of African red slip ware (3rd-7th c.) in Northern and Central Tunisia: Archaeological provenance and reference groups based on chemical analysis. *Journal of Roman Archaeology*, 15, 121–158.
- Maggetti, M. (2001). Chemical analyses of ancient ceramics: What for? *Chimia*, 55, 923–930.
- Maniatis, Y., & Tite, M. S. (1981). Technological examination of Neolithic-Bronze Age pottery from central and southeast Europe and from the Near East. *Journal of Archaeological Science*, 8, 59–76.
- Maritan, L., Angelini, I., Artioli, G., Mazzoli, C., & Saracino, M. (2009). Secondary phosphates in the ceramic materials from Frattesina (Rovigo, North-Eastern Italy). *Journal of Cultural Heritage*, 10, 144–151.
- Maritan, L., & Mazzoli, C. (2004). Phosphates in archaeological finds: Implications for environmental conditions of burial. *Archaeometry*, 46, 673–683.
- Maritan, L., Nodari, L., Mazzoli, C., Milano, A., & Russo, U. (2006). Influence of firing conditions on ceramic products: Experimental study on clay rich in organic matter. *Applied Clay Science*, 31, 1–15.
- Martucci, C. S., Boemio, G., Trojsi, G., & De Simone, G. F. (2012). Pollena Trocchia (NA), località Masseria De Carolis. L'analisi dei reperti per la ricostruzione del contesto economico e sociale della villa romana. *Amoenitas II*, 87–117.
- Martucci, C. S., Germinario, C., Grifa, C., De Simone, G. F., Langella, A., Cappelletti, P., & Morra, V. (2018). Late Roman Slipped or Painted wares? Technology and chronology of some Campanian productions. In D. Delphine (Ed.), *LRCW-5, Late Roman coarse wares, cooking wares and amphorae in the Mediterranean—Archaeology and archaeometry* (pp. 347–358). Alexandria: Centre d'Études Alexandrines.
- Martucci, C. S., De Simone, G. F., & D'Italia, S. (2014). Local productions around Vesuvius: Trade patterns and identity. *Rei Cretariae Romanae Fautorum Acta*, 43, 433–442.
- Melluso, L., de' Gennaro, R., Fedele, L., Franciosi, L., & Morra, V. (2012). Evidence of crystallization in residual, Cl-F-rich, agpaite, trachyphonolitic magmas and primitive Mg-rich basalt-trachyphonolite interaction in the lava domes of the Phlegrean Fields (Italy). *Geological Magazine*, 149, 532–550.
- Mercurio, M., Bish, D. L., Cappelletti, P., De'Gennaro, B., De'Gennaro, M., Grifa, C., ... Langella, A. (2016). The combined use of steam-treated

- bentonites and natural zeolites in the oenological refining process. *Mineralogical Magazine*, 80, 347–362.
- Mioč, U. B., Colombari, P., Sagon, G., Stojanović, M., & Rosić, A. (2004). Ochre decor and cinnabar residues in Neolithic pottery from Vinča, Serbia. *Journal of Raman Spectroscopy*, 35, 843–846.
- Molera, J., Pradell, T., & Vendrell-Saz, M. (1998). The colours of Ca-rich ceramic pastes: Origin and characterization. *Applied Clay Science*, 13, 187–202.
- Morimoto, N. (1988). Nomenclature of pyroxenes. *Mineralogy and Petrology*, 39, 55–76.
- Mukay, T., & Aoyagi, M. (2014). Un contexte de la fin du IIIe s. à Somma Vesuviana (Campanie, Italie). In N.Poulou-Papadimitriou & E. V. Nodarou (Eds.), *LRCW 4, Late Roman Coarse Wares, Cooking Wares and Amphorae in the Mediterranean: Archaeology and archaeometry. The Mediterranean: A market without frontiers* (Vol. 1, pp. 864–871). Oxford: BAR International Series 2616 I, Archeopress.
- Nodari, L., Marcuz, E., Maritan, L., Mazzoli, C., & Russo, U. (2007). Hematite nucleation and growth in the firing of carbonate-rich clay for pottery production. *Journal of the European Ceramic Society*, 27, 4665–4673.
- Nodari, L., Maritan, L., Mazzoli, C., & Russo, U. (2004). Sandwich structures in the Etruscan-Padan type pottery. *Applied Clay Science*, 27, 119–128.
- NORMAL 29/88. (1988). *Misura dell'indice di asciugamento (drying index)*. Roma: CNR-ICR.
- NORMAL 7/81. (1981). *Assorbimento d'acqua per Immersione Totale-Capacità di Imbibizione*. Roma: CNR-ICR.
- Peña, J. T., & McCallum, M. (2009a). The production and distribution of pottery at Pompeii: A review of the evidence; part 1, production. *American Journal of Archaeology*, 113, 57–79.
- Peña, J. T., & McCallum, M. (2009b). The production and distribution of pottery at Pompeii: A review of the evidence; part 2, the material basis for production and distribution. *American Journal of Archaeology*, 113, 165–201.
- Quinn, P. S. (2013). *Ceramic petrography: The interpretation of archaeological pottery & related artefacts in thin section*. Oxford: Archeopress.
- R Development Core Team. (2008). *R: A language and environment for statistical computing*. Vienna: R Foundation for statistical Computing.
- Rathossi, C., & Pontikes, Y. (2010). Effect of firing temperature and atmosphere on ceramics made of NW Peloponnese clay sediments. Part I: Reaction paths, crystalline phases, microstructure and colour. *Journal of the European Ceramic Society*, 30, 1841–1851.
- Reedy, C. L., Anderson, J., Reedy, T. J., & Liu, Y. (2014). Image analysis in quantitative particle studies of archaeological ceramic thin sections. *Advances in Archaeological Practice*, 2, 252–268.
- RILEM. (1980). *Recommended tests to measure the deterioration of stone and to assess the effectiveness of treatment methods*. In RILEM TC 25-PEM (Ed.), *Materials and structures* (Vol. 13, pp. 175–253). Bagnex: RILEM Publications SARL.
- Rye, O. S. (1976). Keeping your temper under control: Materials and manufacture of Papuan pottery. *Archaeology and Physical Anthropology in Oceania*, 11, 106–137.
- Santoriello, A., & Siano, S. (2018). Late Roman tableware and cooking ware from ancient Appia landscapes survey (Benevento-Italia). In D.Delphine (Ed.), *LRCW-5, Late Roman coarse wares, cooking wares and amphorae in the Mediterranean - Archaeology and archaeometry* (Vol. 1, pp. 363–383). Alexandria: Centre d'Études Alexandrines.
- Scarpati, C., Perrotta, A., & Luongo, G. (2009). The history of the eruptions on the northern slope of Somma-Vesuvius. In G. F. De Simone & R. T. Macfarlane (Eds.), *Apolline Project vol. 1: Studies on Vesuvius' North Slope and the Bay of Naples* (Vol. 1, pp. 271–278). Napoli: Università degli Studi Suor Orsola Benincasa Napoli–Brigham Young University.
- Scarpati, C., Perrotta, A., & De Simone, G. F. (2016). Impact of explosive volcanic eruptions around Vesuvius: A story of resilience in Roman time. *Bulletin of Volcanology*, 78, 21.
- Scarpelli, R., Clark, R. J. H., & De Francesco, A. M. (2014). Archaeometric study of black-coated pottery from Pompeii by different analytical techniques. *Spectrochimica Acta, Part A: Molecular and Biomolecular Spectroscopy*, 120, 60–66.
- Schwedt, A., & Mommsen, H. (2007). On the influence of drying and firing of clay on the formation of trace element concentration profiles within pottery. *Archaeometry*, 49, 495–509.
- Sendova, M., Zhelyaskov, V., Scalera, M., & Ramsey, M. (2005). Micro-Raman spectroscopic study of pottery fragments from the Lapatsa tomb, Cyprus, ca 2500 BC. *Journal of Raman Spectroscopy*, 36, 829–833.
- Shebanova, O. N., & Lazor, P. (2003). Raman spectroscopic study of magnetite (FeFe₂O₄): A new assignment for the vibrational spectrum. *Journal of Solid State Chemistry*, 174, 424–430.
- Soricelli, G. (2015). *Appunti sulla produzione e circolazione della ceramica tra la Baia di Napoli e la Campania settentrionale tra II e V secolo d.C.* *Analysis Archaeologica*, 1, 185–211.
- Toniolo, L. (2012). *Archeologia del commercio e archeologia del consumo a Napoli nella tarda età imperiale: uno studio archeometrico e storico-economico del vasellame* (Unpublished doctoral dissertation). Università Cà Foscari, Venezia.
- Valanciene, V., Siauciunas, R., & Baltusnikaite, J. (2010). The influence of mineralogical composition on the colour of clay body. *Journal of the European Ceramic Society*, 30, 1609–1617.
- Whitney, D. L., & Evans, B. W. (2010). Abbreviations for names of rock-forming minerals. *AMERICAN MINERALOGIST*, 95, 185–187.
- Wickham, C. (1998). *Economia altomedievale*. In M. Donzelli (Ed.), *Storia medievale* (pp. 203–225). Rome: Manuali Donzelli.
- Wilson, A. I., Schörle, K., & Rice, C. (2012). Roman ports and Mediterranean connectivity. In S. Keay (Ed.), *Portus and the Ports of the Roman Mediterranean (Archaeological Monographs of the British School at Rome)* (Vol. 21, pp. 367–391). London: British School at Rome.

SUPPORTING INFORMATION

Additional supporting information may be found online in the Supporting Information section.

How to cite this article: Germinario C, Cultrone G, De Bonis A, et al. Production technology of late Roman decorated tableware from the Vesuvius environs: Evidence from Pollena Trocchia (Campania region, Italy). *Geoarchaeology*. 2021;36: 34–53. <https://doi.org/10.1002/gea.21819>